

國立交通大學

物理研究所

碩士論文

在液態鎵模型中結構次序之量化

Quantification of structure order in a model of liquid Ga



研究生：陳琳元

指導教授：吳天鳴 教授

中華民國九十九年六月

在液態鎵模型中結構次序之量化
Quantification of structure order in model of liquid Ga

研究生：陳琳元

Student : Lin-Yuan Chen

指導教授：吳天鳴 教授

Advisor : Ten-Ming Wu

國立交通大學

物理研究所

碩士論文



A Thesis

Submitted to Institute of Physics

College of Science

National Chiao Tung University

in partial Fulfillment of the Requirements

for the Degree of

Master

in

Physics

July 2010

Hsinchu, Taiwan, Republic of China

中華民國九十九年六月

在液態鎂模型中結構次序之量化

學生：陳琳元

指導教授：吳天鳴 教授

國立交通大學物理研究所碩士班



爲了量化描述物質結構在影像上資訊的數學參數，包括可以了解整體性的結構次序的 orientational order parameter 和 translational order parameter，可以判別固體堆垛的 local orientational order parameter，我們利用這些參數來探討在不同熱力學狀態下，液態鎂模型的系統結構次序。Orientational order parameter 可以了解整體性的結構次序，translational order parameter 探討系統在長距離內平移性結構次序，而 local orientational order parameter 可探討區域性結構次序，並當成協助判斷固體堆垛的方法。我們探討了在不同溫度、密度下結構參數以及固體堆垛形成，並探討了 Friedel oscillations 的影響。

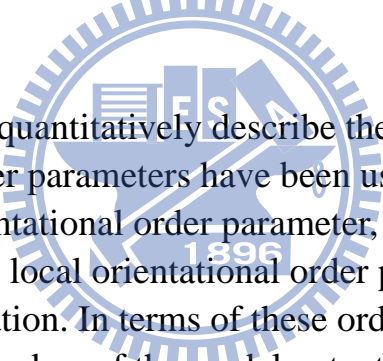
Quantification of structure order in model of liquid Ga

student : Lin-Yuan Chen

Advisors : Dr. Ten-Ming Wu

Institute of Physics
National Chiao Tung University

ABSTRACT



In this thesis, in order to quantitatively describe the structure order in a model of liquid Ga, several order parameters have been used, including translational order parameter and orientational order parameter, which characterize the global structures, and the local orientational order parameter, which is used to analyze the cluster formation. In terms of these order parameters, we investigate the structure orders of the model potential at various thermodynamic states. For the model and the repulsive core only of the model, the variations of these order parameters and the cluster formation with temperature and densities are presented, so that the effects due to the Friedel oscillations are obtained and discussed.

誌

謝

感謝吳天鳴老師在我碩班期間的指導讓我學會很多東西，謝謝我的家人讓我有這個機會來讀碩班，謝謝蔡昆憲學長、黃邦傑學長、黃柏翰學長在寫程式上教會我許多東西，也給了我許多建議，謝謝唐平翰學長給了我許多建議，謝謝鄧德明學長、謝宏慶學長陪我渡過碩班的休閒時間，也跟我一起打球。

感謝碩班同學尤偉任、陳志榮、李傳睿、周禹廷、黃以撒，在我遇到問題以及修課方面提供我不少參考意見，也陪我渡過這兩年碩班時光。



Contents

Abstract (Chinese).....	i
Abstract (English).....	ii
Acknowledgement.....	iii
Content	iv
Figure Captions.....	vi
Chapter 1 Introduction.....	1
Chapter 2 Model of liquid Ga and MD simulation	2
Chapter 3 Static structure factor, Order Parameters and Cluster Analysis	
3-1 Radial distribution function.....	4
3-2 Static structure factor	4
3-3 Translational order parameter.....	5
3-4 Orientational order parameter.....	5
3-5 Local orientational order parameter.....	6
3-5-1 Threshold value for Cluster Formation.....	8
Chapter 4 Numerical Results and Discussions.....	9
4-1 Variation of structures with density at T=323K.....	9
4-1-1 Translational order parameter.....	9
4-1-2 Orientational order parameter.....	9
4-1-3 Order map.....	9
4-1-4 Clusters of Full potential	10
4-1-5 Clusters of Repulsive core only	11
4-2 Variation of structures with temperature at density $\rho = 3.305$	11
4-2-1 Translational order parameter.....	12
4-2-2 Orientational order parameter.....	12

4-2-3 Order map.....	12
4-2-4 Clusters of Full potential	12
4-2-5 Clusters of Repulsive core only	13
Chapter 5 Conclusions.....	14
Reference.....	15



Figure Captions

Figure. 1.	Static structure factor for liquid Ga at 323K $\rho=3.305$1
Figure. 2.	Interatomic pair potential of liquid Ga.....2
Figure. 3.	Repulsive core potential.....2
Figure. 4.	Cubic box with all side length L and N particles inside3
Figure. 5.	Full potential, Isolated particle number variation with density for $K_c=0.5, K_c=0.7$ and $K_c=0.9$8
Figure. 6.	Variation of translational order parameter with density at $T=323K$16
Figure. 7.	Variation of orientational order parameter with density at $T=323K$17
Figure. 8.	(a) Static structure factor of full potential at $T=323K$ (b) Static structure factor of repulsive core only at $T=323K$...18
Figure. 9.	Order maps of full potential (circles) and repulsive core only (squares) at $T=323K$19
Figure. 10.	Cluster distributions of the full potential with $K_c=0.5$ and the cutoff of the bond length at $r_{min}=0.89$20
Figure. 11.	Cluster distributions of the full potential with $K_c=0.5$ and the cutoff of the bond length at $r_{min}=1.1$21
Figure. 12.	Cluster distributions of the full potential with $K_c=0.5$ and the cutoff of the bond length at $r_{min}=1.3$22
Figure. 13.	Cluster distributions of the full potential with $K_c=0.5$ and the cutoff of the bond length at $r_{min}=1.5$23
Figure. 14.	Cluster distributions of the full potential with $K_c=0.5$ and the cutoff of the bond length at $r_{min}=1.76$24
Figure. 15.	Density variation of the isolated particle number for the full potential with the cutoff distance $r_{min}=0.89, 1.1, 1.3, 1.5$ and 1.7625

Figure. 16.	The $g(r)$ function of the full potential at $T=323K$ and different density.....	26
Figure. 17.	Cluster distributions of the repulsive core only with $K_c=0.5$ and the cutoff of the bond length at $r_{min}=0.89$	27
Figure. 18.	Cluster distributions of the repulsive core only with $K_c=0.5$ and the cutoff of the bond length at $r_{min}=1.1$	28
Figure. 19.	The $g(r)$ function of the repulsive core only at $T=323K$ and different density.....	29
Figure. 20.	Distribution of the isolated particles in the full potential (circles) and the repulsive core only (squares) with $r_{min}=0.89$ (a) and $r_{min}=1.1$ (b).....	30
Figure. 21.	Temperature variation of the translational order parameter at $\rho=3.305$ for the models of the full potential (circles) and the repulsive core only (squares).....	31
Figure. 22.	Temperature variation of the orientational order parameter at $\rho=3.305$ for the models of full potential (circles) and the repulsive core only (squares).....	32
Figure. 23.	Static structure factors $S(q)$ of the full potential (a) and the repulsive core only (b) at $\rho=3.305$	33
Figure. 24.	Order maps for the models of the full potential (circles) and the repulsive core only (squares) at $\rho=3.305$ for several temperatures.....	34
Figure. 25.	Comparison for the order map of the temperature and density variations for the models of the full potential and the repulsive core only.....	35
Figure. 26.	Comparison for the radial distribution functions $g(r)$ of the solids obtained by different simulation process.....	36
Figure. 27.	The cluster distributions of the full potential at $\rho=3.305$ and	

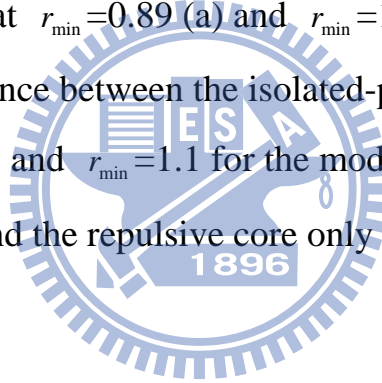
three temperatures with the cutoff $r_{\min}=0.89$ (a) and $r_{\min}=1.1$ (b)
37

Figure. 28. The cluster distributions of the repulsive core only at $\rho=3.305$
 and three temperatures with the cutoff $r_{\min}=0.89$ (a) and
 $r_{\min}=1.1$ (b).....38

Figure. 29. The $g(r)$ function of the full-potential model at $\rho=3.305$ and
 $T=313\text{k}, 283\text{K}, 173\text{K}, 153\text{K}$ and 103K39

Figure. 30. Temperature variation of the isolated-particle distribution for the
 full potential (circles) and the repulsive core only (squares) with
 the cutoff at $r_{\min}=0.89$ (a) and $r_{\min}=1.1$ (b).....40

Figure. 31. The difference between the isolated-particle distribution
 at $r_{\min}=0.89$ and $r_{\min}=1.1$ for the models of the full potential
 (circles) and the repulsive core only (squares).....41



Chapter 1

INTRODUCTION

As one of the polyvalent liquid metals that are well known for anomalous structures, Ga has many uncommon properties, such as low melting point at $T_m=302\text{K}$, and a shoulder on the high- q side of first peak of static structure factor, as shown in Fig.1. The physical reason for this anomalous shoulder is still unknown and gives rise to our curiosity.

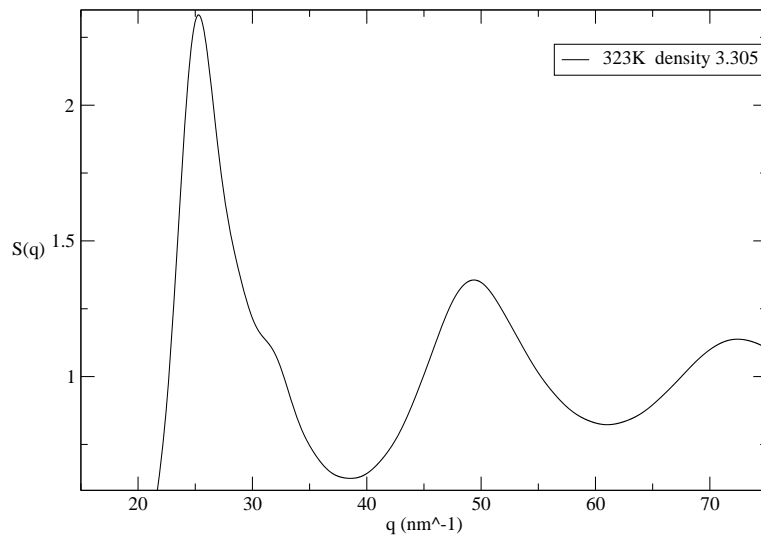


Fig.1 Static structure factor for liquid Ga at 323K $\rho=3.305$

The high- q shoulder can be produced by a model of interatomic pair potential that is generated by a first-principles theory Ref[1]. The interatomic pair potential includes a repulsive soft core and a long-range oscillatory part, called “Friedel oscillations”. It is concluded that the high- q shoulder may be caused by many “1201 clusters”. From Ref[2], we know that for the potential with the repulsive soft core only, the high- q shoulder does not appear.

To find out the cause for the high- q shoulder, we need to know more about the potential model in Ref[1] for pure Ga liquid metal and the effect caused by Friedel oscillations on the structure order of the liquid. Computer simulation results of Ga produce complex structural information, so we use the structure order parameters that are introduced in Ref[3], Ref[4] and Ref[5] to study pure Ga liquid structure. The structure order parameters are a more objective way for describing structure order quantitatively.

Chapter 2

Model of liquid Ga and MD simulation

The effective interatomic pair potential $\phi(r)$ of liquid Ga is generated by a first-principles pseudopotential theory Ref[1] and Ref[6]. The potential model contains a repulsive soft core and an oscillatory tail called “Friedel Oscillations”. As shown in Fig. 2, the minimum of the first attractive well is located at 4.32 Å, and first, second and third maxima are located at 5.17Å, 7.15Å, 9.13Å, respectively. Shown in Fig. 3 is another pair potential that we simulate, and is called “the repulsive-core potential”, which is the repulsive soft core of $\phi(r)$ only. By comparing the simulated results of the two potentials, we can get the effects of the Friedel oscillations in $\phi(r)$.

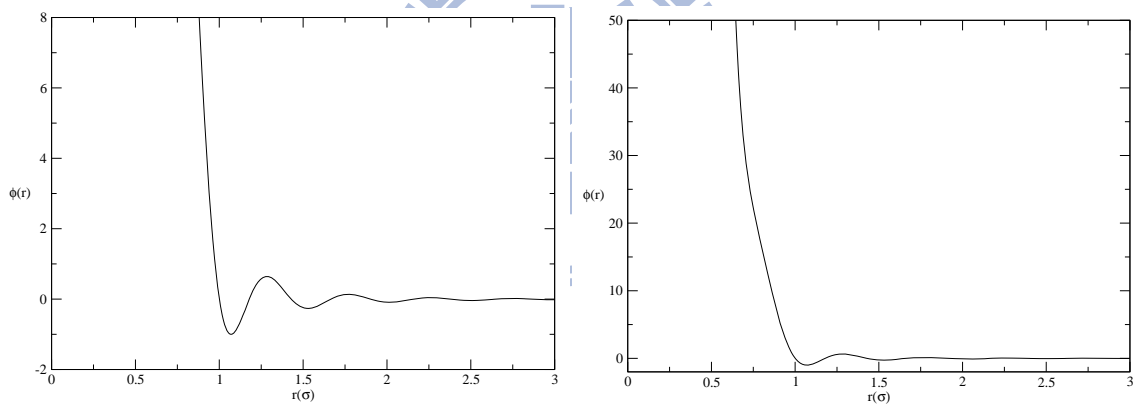


Fig. 2 Interatomic pair potential of liquid Ga

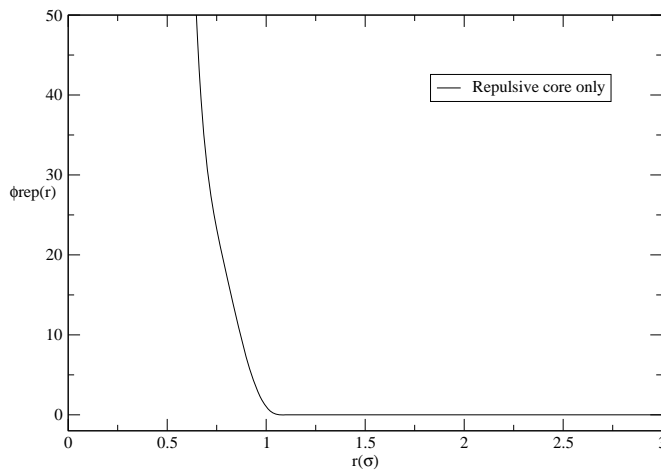


Fig. 3 Repulsive-core potential

Using classical molecular dynamics simulation (MD) and the standard periodic boundary conditions, we simulate N particles interacting with the effective interatomic pair potential $\phi(r)$ or the repulsive core potential $\phi_{\text{rep}}(r)$ in a cubic box of length L under constant temperature T (canonical ensemble) with Verlet algorithm Beeman form.

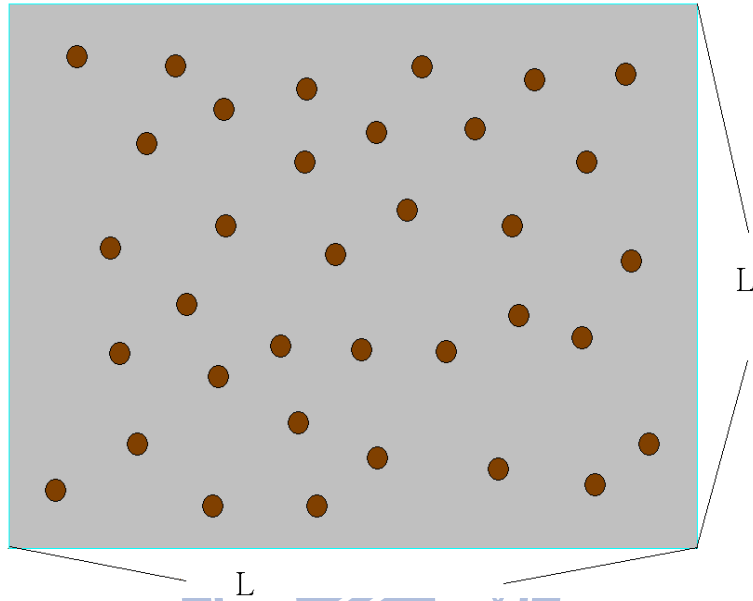


Fig. 4 Cubic box with all side length L and N particles inside

In the first part MD with $T=323\text{K}$, we get configurations of system at different densities. The temperature 323K is slightly above the melting temperature of Ga, so that we can study structures in liquid states. As density increases, the system may be change to a solid state at 323K .

In the second part, the reduced density of the system is fixed at 3.305 , which is that of Ga at 323K . We get system configurations at different temperatures.

In our simulations, $\sigma = 7.645 \text{ au} = 4.044 \text{ \AA}$, $t_0 = 5.4 \times 10^{-12} \text{ s} = 5.4 \text{ ps}$, r^* is real distance rescaled by σ , and the time step is $0.001t_0$.

Chapter 3

Static structure factor, Order Parameters and Cluster Analysis

3-1. Radial distribution function[PDF, denoted by g(r)]

The radial distribution function (PDF) describing the structures of configuration is calculated as

$$g(r) = \frac{\Delta n}{\rho \cdot \left(\frac{4}{3}\pi(r^3 - (r - dr)^3)\right)} \quad (1)$$

where ρ is density, Δn is the number of particles that are found between distance r and $r-dr$ from a central particle. Also, $g(r)$ needs to satisfy

$$\int_0^{\infty} \rho * g(r) * 4\pi r^2 * dr \approx N \quad (2)$$

and

$$local_density = g(r) * \frac{N}{V} = \frac{\Delta n}{\frac{4}{3}\pi(r^3 - (r - dr)^3)} \quad (3)$$

where N is the total number of particles in the system. $g(r)$ is the local density that the central particle feels at distance r . As r is vary large, we have $g(r)=1$, that means the local density from the central particle equals the density of the system.

3-2. Static structure factor

To introduce static structure factor, $S(q)$, we may compare our simulation data with the scattering experimental data. From references, $S(q)$ is defined as

$$S(q) = 1 + \int d\vec{r} \exp(i\vec{k} \cdot \vec{r}) \rho \times (g(r) - 1) \quad (8)$$

3-3. Translational order parameter

Although PDF can show the radial behavior of our system, but to give a quantitative expression for structure order, we introduce translational order parameter defined as

$$\tau = \frac{1}{s_c} \int_0^{s_c} |g(s) - 1| ds \quad (4)$$

where $s = r \cdot \rho^{1/3}$ and $g(s) = g(r\rho^{1/3})$, with $\rho = \frac{N}{V}$ the number density. As r is scaled with the mean separation of particles, the translational order parameter can avoid the effects due to system density. s_c is a numerical cutoff, and we set s_c to be 2.317851 in our calculation.

For a completely uncorrelated system, $g(s)$ is 1 and thus τ vanishes to zero, but for systems with long-range order, τ is very large.

3-4. Orientational order parameter

As the translational order parameter describes the long-range order of structures, we introduce orientational order parameter to describe short-range order of structures. For describing short-range order, we need to define the bonds between particles. The unit vector \hat{r}_{ij} representing the direction pointing from the i -th to the j -th particle is specified by the related polar and azimuthal angles θ_{ij} and ϕ_{ij} . To characterize the bond angles, we use spherical harmonic functions $Y_{lm}(\theta_{ij}, \phi_{ij})$,

$$Y_{lm}(\theta, \phi) = \sqrt{\frac{(2l+1)(l-m)!}{4\pi(l+m)!}} P_l^m(\cos \theta) e^{im\phi} \quad (5)$$

where $P_m^l(x)$ is the associated Legendre function. The purpose of orientational order parameter is to quantify short-range order; therefore, a cutoff distance r_{\min} is required. r_{\min} is usually set as the first minimum position of $g(r)$, to include the particles within the first-shell structure of a central particle. For a central particle “i” and n_i particles within the cutoff distance r_{\min} ,

$$\overline{Q_{lm}} = \frac{1}{N_{bond}} \sum_{i=1}^N \sum_{j>i}^{n_i} Y_{lm}(\theta_{ij}, \phi_{ij}) \quad (6)$$

is the average of bond spherical harmonic functions, with N_{bond} being the total number of bonds with central particles. To avoid the effects due to the coordinate axes we choose, a rotationally invariant order parameter Q_l is then an average square sum of different m in Eq.(6) as

$$Q_l = \sqrt{\frac{4\pi}{2l+1} \sum_{m=-l}^l |\overline{Q_{lm}}|^2} \quad (7)$$

In this work, we use Q_6 , which decreases as the system becomes less structural, and increases as the system structure is crystal-like. For example, for a perfect fcc crystal with 12 first nearest neighbors, $Q_6^{fcc} = 0.5745$, and for a completely uncorrelated system, $Q_6 = \frac{1}{\sqrt{N_{bond}}}$.

3-5. Local orientational order parameter

We define the local orientational order parameter for determining clusters.

For particles within the bond length r_{\min} , we sum the spherical harmonic function of bonds to the i -th particle as

$$\overline{q_{lm}}(i) \equiv \frac{1}{n_i} \sum_{j=1}^{n_i} Y_{lm}(\theta_{ij}, \phi_{ij}) \quad (9)$$

where n_i is the local bond number to the i -th particle. Like what we have done for the orientational order parameter, one can evaluate a rotationally invariant order parameter that quantifies the local structure order associated with the i -th particle as

$$q_l(i) \equiv \left[\frac{4\pi}{2l+1} \sum_{m=-l}^l |\overline{q_{lm}}(i)|^2 \right]^{1/2} \quad (10)$$

Choose $l=6$ for our work. Therefore, any particles in the system have a complex vector of $2 \times 6 + 1$ components characterizing the local structure order, with each component as

$$\tilde{q}_{6m}(i) \equiv \frac{\overline{q_{6m}}(i)}{\sqrt{\sum_{m=-6}^6 |\overline{q_{6m}}(i)|^2}} \quad (11)$$

The properties of vector-dot product are that for any two normalized vectors in the same direction, their dot product equals 1. For two particles i and j within the r_{\min} range, with the local orientational order parameter vector-dot product is greater than a threshold value K_c ,

$$q_6(i) \bullet q_6(j) \equiv \sum_{m=-6}^6 \tilde{q}_{6m}(i) \tilde{q}_{6m}(j)^* > K_c \quad (12)$$

we say that the two particles i and j are “Connected”. A cluster is a group of connected particles. So, we use the connect relation between particles to find clusters and determine their sizes. A particle without any connected particles is called an isolate particle, which does not belong to any group clusters.

3-5-1. Threshold value for Cluster Formation

If threshold value K_c of local orientational order parameter is too small, the effect structure order for distinguishing will be low Ref[5]. The results of different threshold values K_c for calculating local orientational order parameter are shown in Fig. 5. For $K_c=0.9$ and 0.7 , very few bonds can be recognized, and most particles are classified as “isolate particle”(without connected neighbors). Thus, we choose $K_c=0.5$ in our study so that the cluster number is clearly varied with system density.

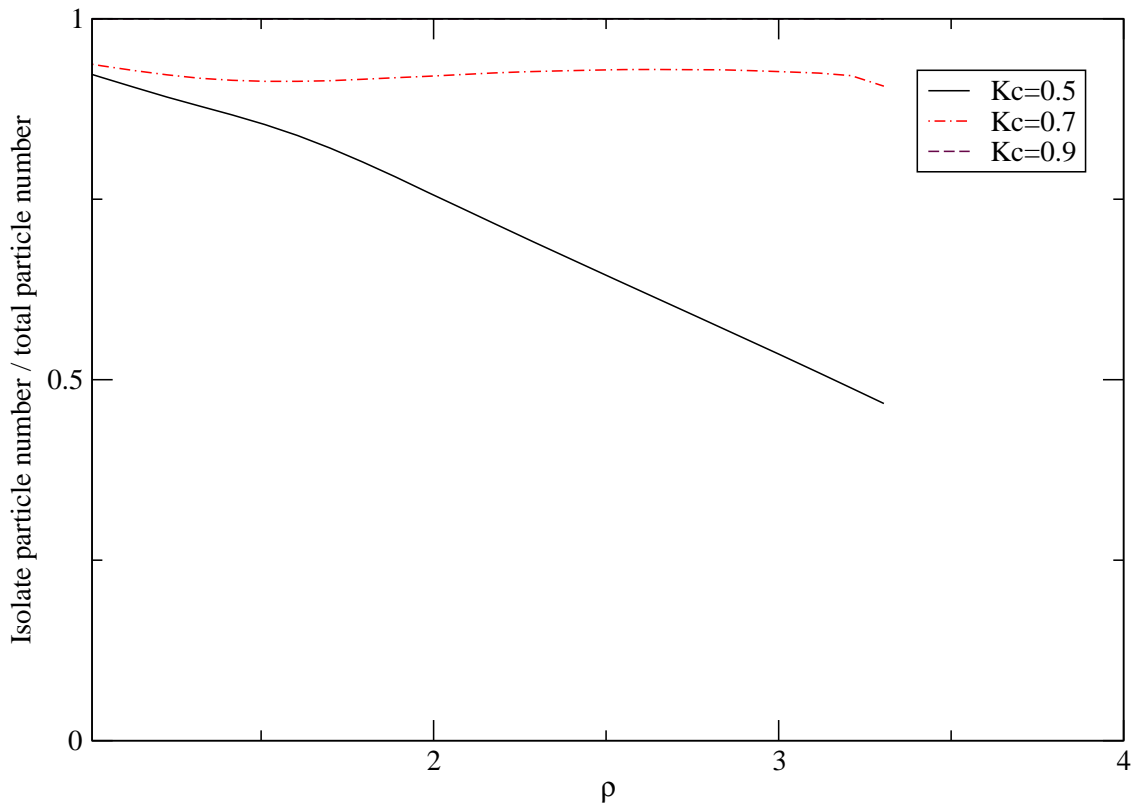


Fig. 5 Isolate-particle number variation with density at $K_c=0.5$, $K_c=0.7$ and $K_c=0.9$, for the system of full potential.

Chapter 4

Numerical Results and Discussions

4-1 Variation of structures with density at T=323K

In this subsection, we examine the variation of simulation results with density of temperature 323K. The translational order parameter τ shown in Fig. 6 and orientational order parameter Q_6 in Fig. 7 have the same behavior as in Ref[4]. From $g(r)$ in Fig.16 (f) and $S(q)$ Fig. 8 with Ref[5], Ref[6], we know that our system changes to a glassy state, as the discontinuous jump occurs in the density variations of τ , Q_6 and in the order map.

4-1-1 Translational order parameter

Fig. 6 is the quantitative results of the translational order parameter. Both Full potential and Repulsive core only show the same behavior that τ increases with density. For systems at low density, the full-potential system is a little more order than the repulsive-core-only system. At high densities, the repulsive-core-only system is a little more order than the full-potential system. τ has a discontinuous jump at density about 4. We know from Ref[3],Ref[4] the jump corresponds to the system phase transition from liquid to solid state. This can also be observed from $g(r)$ in Fig. 16. At solid states, the translational order parameter of full potential is higher than that of the repulsive core only, which shows that Friedel oscillations have a positive effect on the translational order of the structure.

4-1-2 Orientational order parameter

At liquid states, bond orientation of particles are out of order, as in Fig. 7, and the Q_6 value is vary small. At density about 4, Q_6 has a discontinuous jump as that in the translational order parameter. As the system transfers to the solid state, the bond-orientational order is significantly increased, and we can see from Fig. 7 the Q_6 of the full potential is higher than that of the repulsive core only. This also shows that Friedel oscillations of the full potential have a positive effect on the structure order in the solid states.

4-1-3 Order map

Fig. 9 shows order map of translational order parameter versus Q_6 . The results the full potential and the repulsive core only are almost the same at

liquid states. In the order map, the solid states are separated from the liquid states. In the solid states, the structures of the full potential are more order in Q_6 than those of the repulsive core only.

4-1-4 Clusters of Full potential

Fig. 10, Fig 11, Fig. 12, Fig. 13, and Fig. 14 show the distributions of cluster sizes for the full potential with different r_{\min} cutoffs. In Fig. 10 with the cutoff at $r_{\min}=0.89$, only the first shell of $g(r)$ shown in Fig. 16 is taken into account. The size of a cluster and the number of clusters increase as density is increased, as our expectations. From Fig. 16, the first peak of $g(r)$ grows exactly with density. In Fig. 11 with $r_{\min}=1.1$, this cutoff includes the second shell in $g(r)$ that is very close to the first shell of structure, and the clusters keep growing with the increase of density. But at density about 1.8 to 2.6, the cluster distributions are almost the same. This is resulted from the second peak in $g(r)$ lower and the first peak higher, because in this density range the second shell structure starts to be compressed into the first shell and the two shells of structure merge into one. Also from Fig. 6 at the same density region, the translational order parameter is close to be horizontal, which means that the radial structure order of the system does not increase. In Fig. 12, with $r_{\min}=1.3$, the distribution of clusters still has a tendency to grow with density. As density is over 2.8 because part of the third shell as shown in $g(r)$ is included, the clusters grow strongly. But at densities between 1.6 and 2.4, clusters have an anomaly behavior with the local structure order decreasing as density increases. The reason of this behavior is that in this density region as density increases, part of the second shell of the structure is destroyed and classified into different group of the first shell and the third shell. As we can see that the third-shell peak in Fig. 16 gets close to 1.3 but just at the range out of 1.3. In Fig. 13 with $r_{\min}=1.5$, again, the clusters grow with density. For density over 1.7, almost all of the third shell structure are counted in, and thus the clusters become vary large. In Fig. 14 with $r_{\min}=1.76$, the cluster behavior is generally proportional to density. Almost all of the particles in system are recognized as a big cluster. By considering the results of above and Fig. 15 for

the isolate-particle distribution at different densities and cutoffs, a large r_{\min} will cause a difficulty in comparing the results. Therefore, we take $r_{\min} = 0.89$ and $r_{\min} = 1.1$ for the works of different potential Ga model simulation and temperature variation for the full potential and the repulsive core only Ga model simulation. We can see in $g(r)$, $r_{\min} = 0.89$ is the position that contains the first shell of the structure, and $r_{\min} = 1.1$ contains the second shell so that we can know the local order by these two cutoff distances.

4-1-5 Clusters of Repulsive core only

In Fig. 17 and Fig. 18 we show simulation results of the cluster distributions of the repulsive core only at $r_{\min} = 0.89$ and $r_{\min} = 1.1$, respectively. In Fig. 20, the distribution of isolate particles, which are particles do not connect with any other particles are compared for the two pair potentials we simulated. If the isolate-particle number is higher, the structure is less order. For $r_{\min} = 1.1$ and density between 2 and 2.7, as density increases, the cluster structures do not follow. This happens to the cases with the full potential and the repulsive core only, because at $r_{\min} = 1.1$, the system can not distinguish the second shell from the first shell.

Shown in Fig. 20, we find that for low densities the full-potential model has higher local-structure order than the repulsive core only, and for high densities the situation is reversed. The difference between the two cases should be caused by the Friedel oscillations in the full potential. From $g(r)$ and $S(q)$ for the full potential and the repulsive core only we can see that the main reason that causes the system turn into solid states should be the repulsive core part of the potential, because both models turn into solid states at density about 4.

4-2 Variation of structures with temperature at density $\rho = 3.305$

In this subsection, we examine the variation of the simulated structures with temperature at $\rho = 3.305$. The temperature variations of the translational order

parameter τ and the orientational order parameter Q_6 are shown in Fig. 21 and Fig. 22, respectively. For the full potential, as temperature decreases a jump of τ and Q_6 appears, similar as the one as the density of the system increase. Compared with $S(q)$ shown in Fig. 23, we show the solid state similar as the β -phase of Ga. This evidences that our temperature variation MD simulation is correct.

4-2-1 Translational order parameter

The translational order parameter tends to grow very little as temperature is decreased. However, as temperature is lower than about 150K, the system of full potential turns to solids. This can also be evidenced from $g(r)$. We observe that τ has a discontinuous jump. But, for the repulsive core, the translational order parameter does not have a discontinuous jump. The main reason that the system of the full potential turns to solid in the quenching process should be due to the Friedel oscillations of the full potential.

4-2-2 Orientational order parameter

For Q_6 in Fig. 22, again, the full potential has a discontinuous jump similar as one in the translational order parameter. From the behavior of these two order parameters and $g(r)$ in Fig. 29, we clearly show the repulsive core only does not turn to solid state. The result of Q_6 also supports the reason that causes system of the full potential turning to a solid in the quenching process should be the Friedel oscillations of the full potential.

4-2-3 Order map

Fig. 24 shows that the order map of the repulsive core only is almost a straight line because it does not turn to a solid state. But, the order map of the full potential jumps into the top-right part of the figure as the structures changes to a solid.

We put the order maps of different processes together in Fig. 25 and compare the $g(r)$ of the corresponding solid states in Fig. 26, which show that different processes are resulted into different solids.

4-2-4 Clusters of Full potential

Shown in Fig. 27 and Fig. 29, as the system temperature quenches from

liquid Ga to β -phase Ga, the first peak in $g(r)$ and the cluster numbers grow. But, the temperature effect is very small.

4-2-5 Clusters of Repulsive core only

We consider the distribution of the isolated particles for the two potential models. For Fig. 30 in the liquid state, the isolate-particle number of the full potential is higher than that of the repulsive core only. According to Ref[1], the high-q-side shoulder in $S(q)$ of Ga maybe caused by many “1201 cluster”. If the number of the “1201 clusters” increases, the bond length between 0.89 and 1.1 will also increase. We compare the cluster number with the cutoff at

$r_{\min}=0.89$ and $r_{\min}=1.1$. In Fig. 31, the number of different between $r_{\min}=0.89$

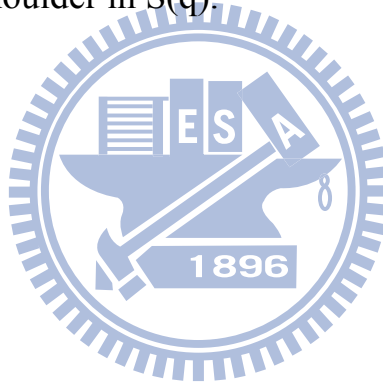
and $r_{\min}=1.1$ for the full potential indeed grows, for the repulsive core only,

the number difference is almost constant. From $S(q)$ of the full potential case, the high-q shoulder grows up, but for the repulsive core only, $S(q)$ does not have the shoulder, this agrees with Ref[1] that the high-q shoulder is cause by many “1201 clusters”. From $g(r)$ and $S(q)$ of both the full potential and the repulsive core only, we can see that the main reason that causes the system turning into solids in the temperature-quench process should be Friedel oscillations of the potential, so that the repulsive core only, the system does not turn to solids in the quenching process.

Chapter 5

Conclusions

According to the results of our simulations, phase transition can be easily observed with the translational order parameter and the orientational order parameter that we use to describe structure order. Different potentials and different processes in simulations produce different paths in order map. So, we can distinguish different conditions that we use in simulation. Friedel oscillations cause high-density liquid systems with structures less order, but give positive effects on structure order for the system in solid states. The main cause for the high-density solids is the repulsive core of the potential, but the quenched solid is mainly caused by Friedel oscillations of the potential. Our results agree with Ref[1], that “1201 clusters” are the major physical reason for causing the high-q shoulder in $S(q)$.



Reference

- [1] S.F. Tsay, S. Wang, Phys. Rev. B **50** 108 (1994)
- [2] K. H. Tsai, T. M. Wu, and S. F. Tsay, J. Chem. Phys. **132**, 034502 (2010)
- [3] A.B. de Oliveria, P. A. Netz, J. Chem. Phys. **125**, 124505 (2006)
- [4] J.R. Errington and P.G. Denedetti, J. Chem. Phys. **118**, 2256 (2003)
- [5] 黃盈靜，「在 LJ $2n-n$ 系統內結構次序之量化」，國立交通大學，碩士論文，民國 97 年。
- [6] S. F. Tsay, Phys. Rev. B **50**, 103 (1994)
- [7] K. H. Tsai and T. M. Wu, J. Chem. Phys. **129**, 024503 (2008)
- [8] K. H. Tsai, T. M. Wu, S. F. Tsay, and T. J. Yang, J. Phys. Condens. Matter, **19**, 205141 (2007)
- [9] M. P. Allen and D. J. Tyndesly, *Computer Simulation of Liquids* (Clarendon, Oxford, 1987)

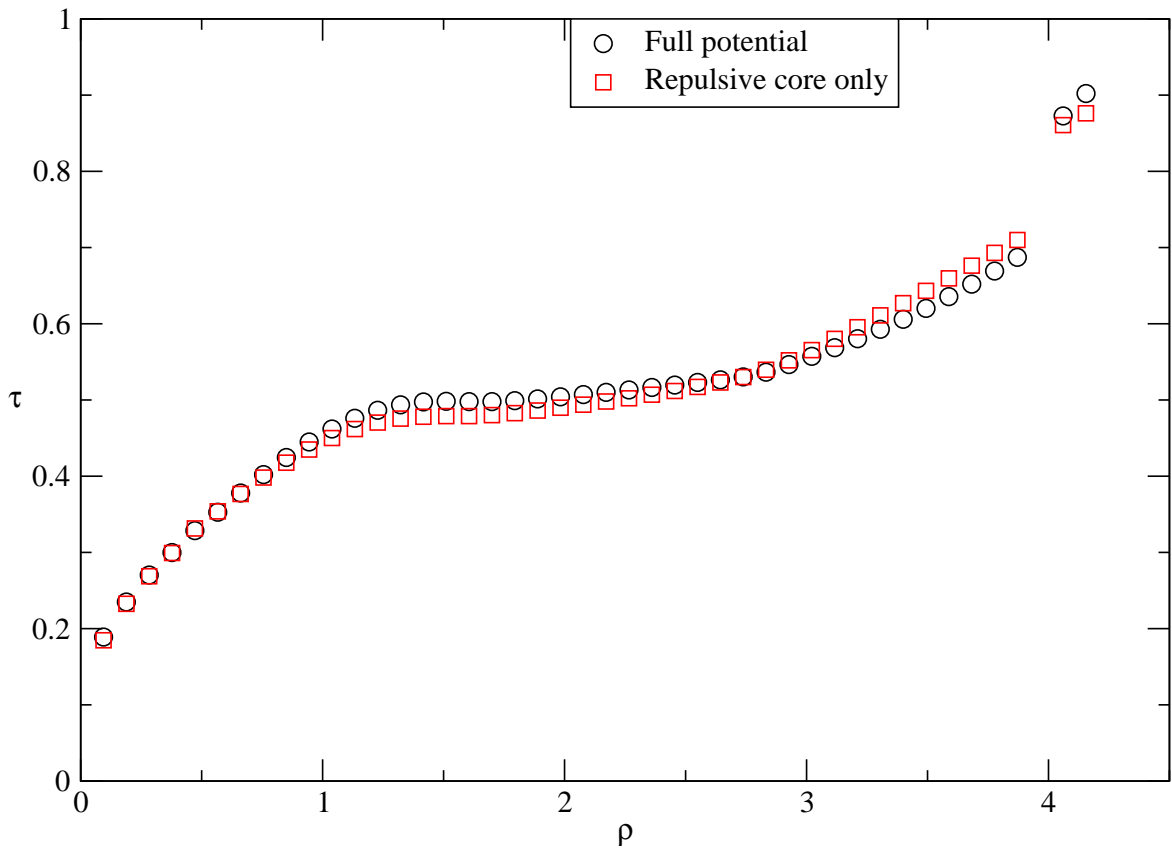


Fig. 6 Variation of translational order parameter with density at T=323K

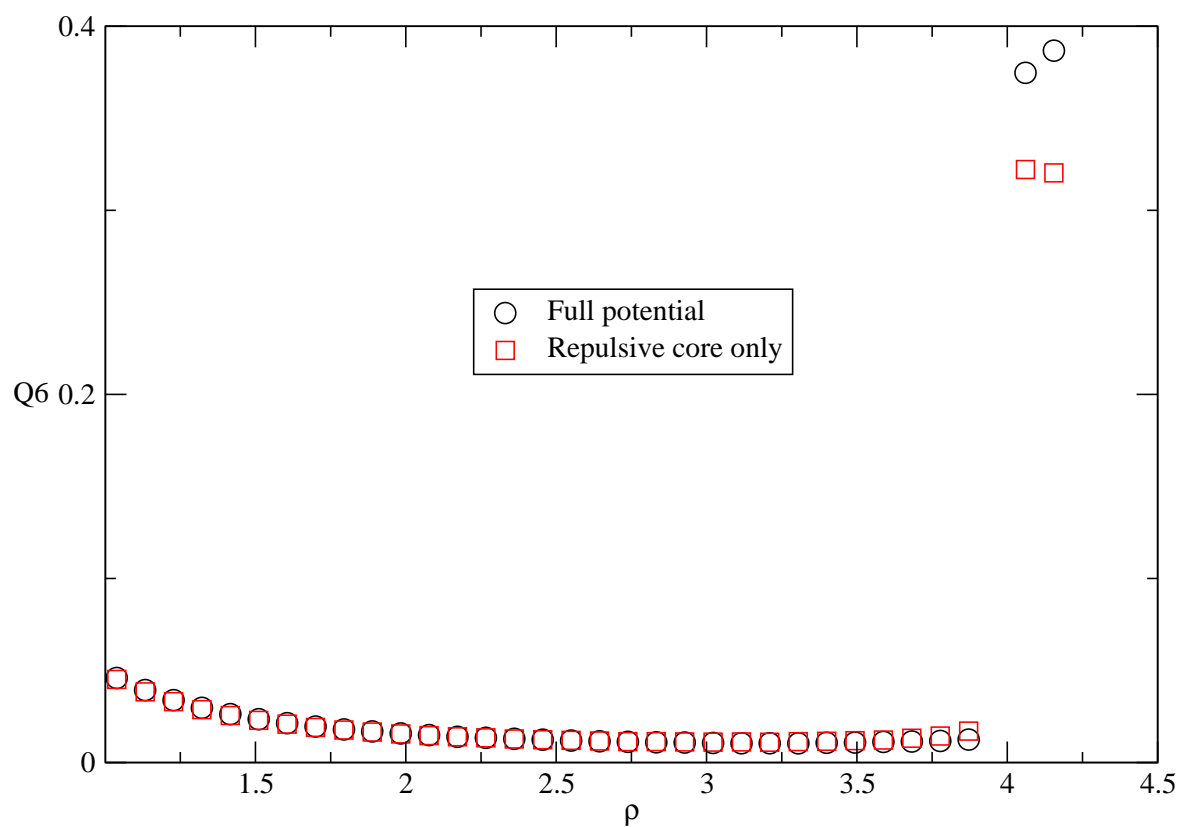


Fig. 7 Variation of orientational order parameter with density at T=323K

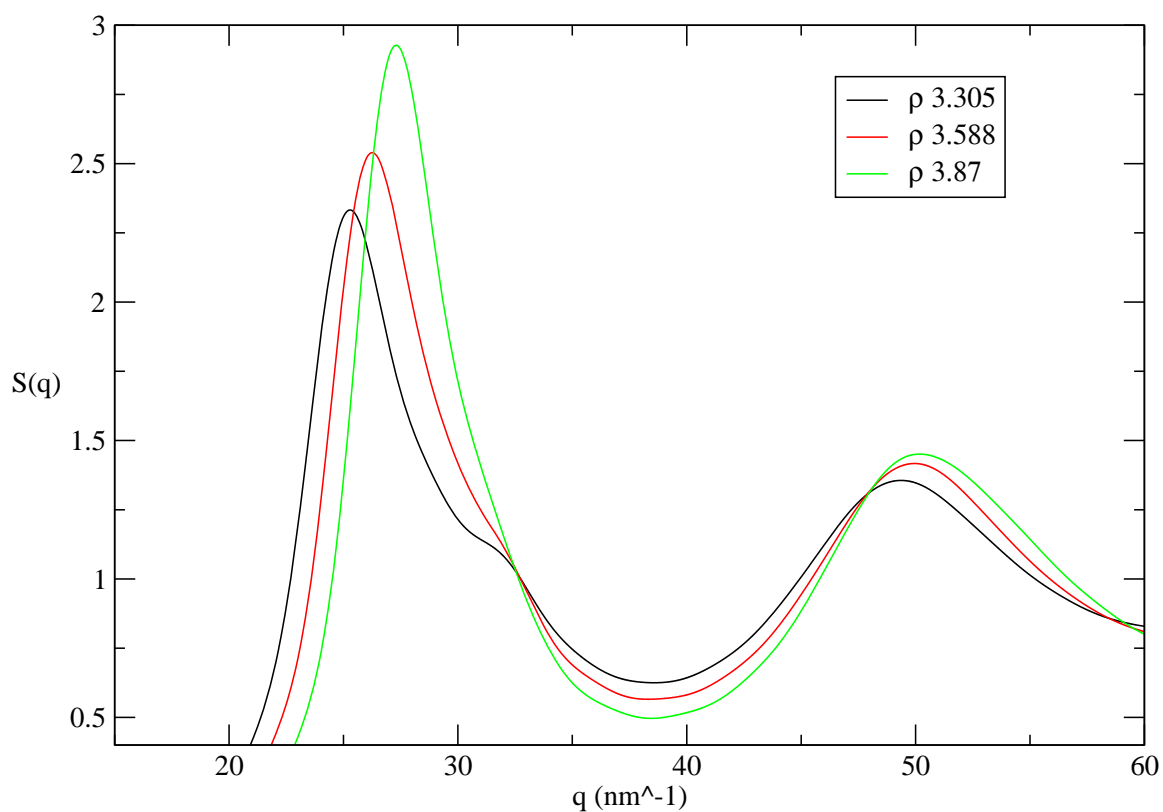


Fig. 8(a) Static structure factor $S(q)$ of full potential at $T=323\text{K}$

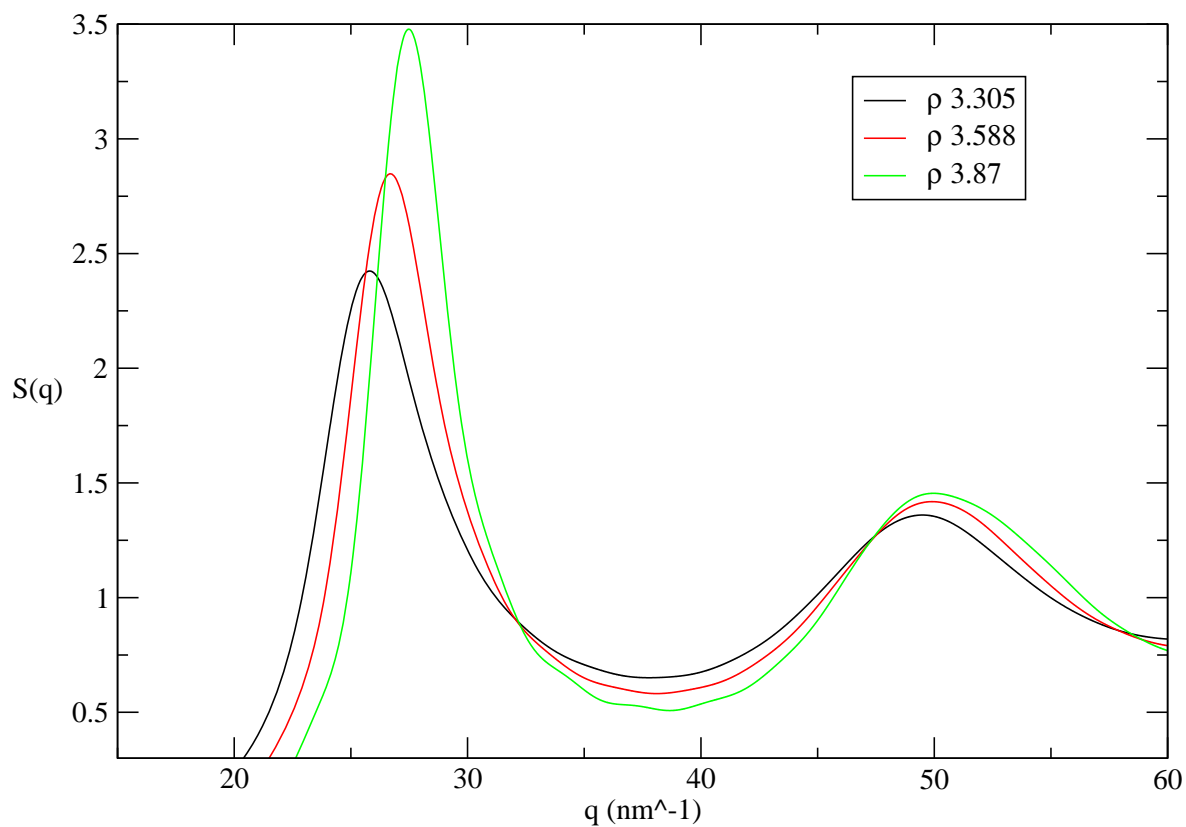


Fig. 8(b) Static structure factor $S(q)$ of repulsive core only at $T=323\text{K}$

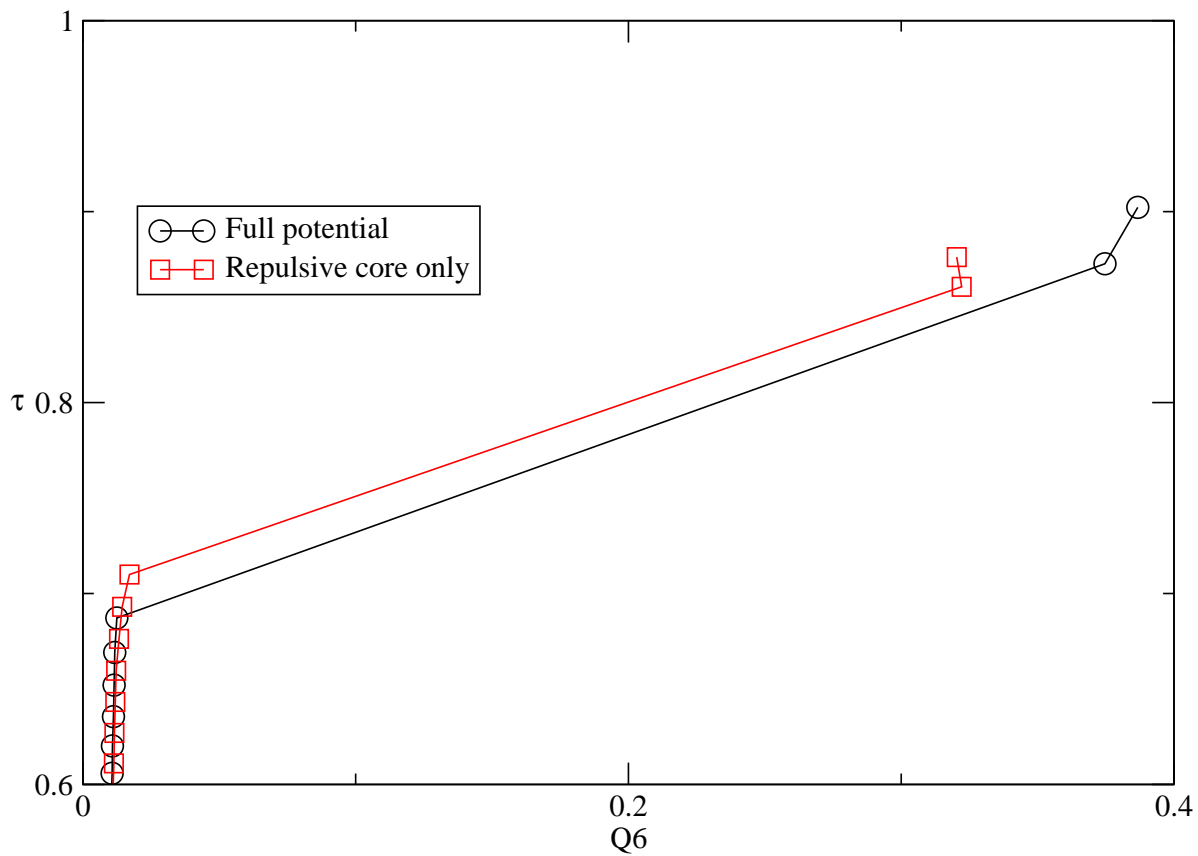


Fig. 9 Order maps of full potential(circles) and repulsive core only(squares) at T=323K

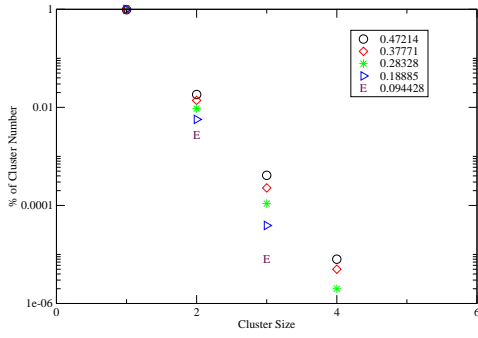


Fig.10 (a)

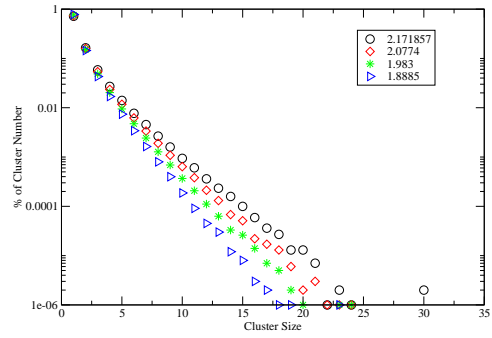


Fig. 10 (e)

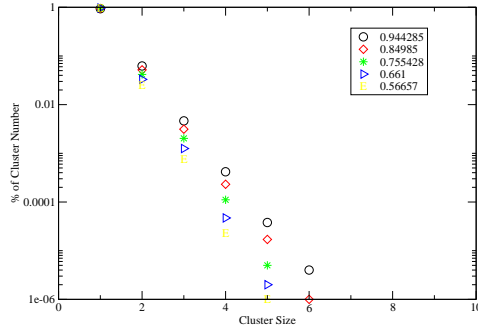


Fig. 10 (b)

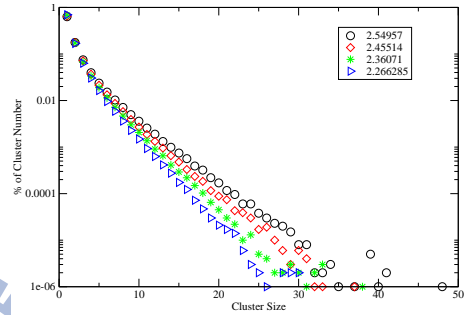


Fig. 10 (f)

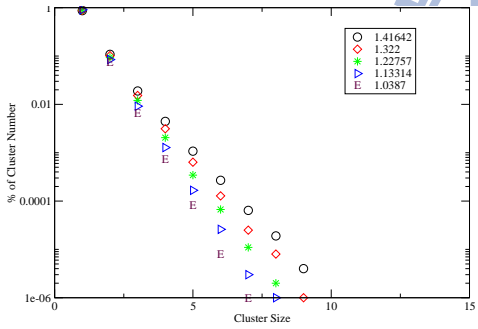


Fig. 10 (c)

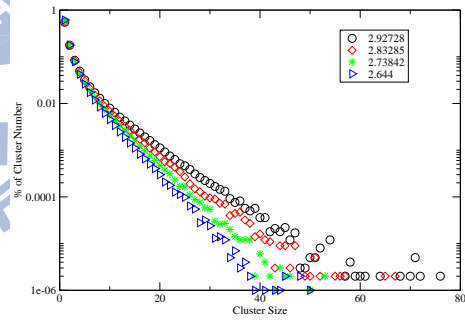


Fig. 10 (g)

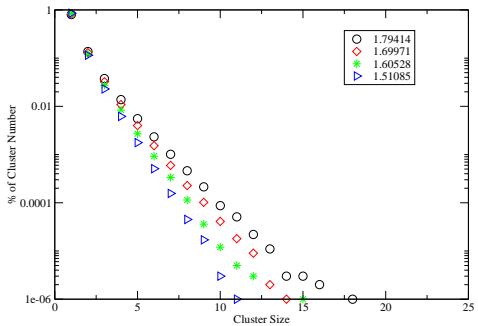


Fig. 10 (d)

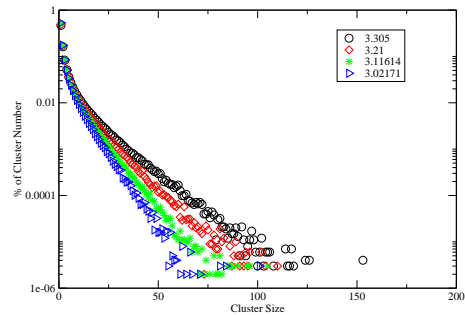


Fig. 10 (h)

Fig.10 Cluster distributions of the full potential with $K_c=0.5$ and the cutoff of the bond length at $r_{\min}=0.89$

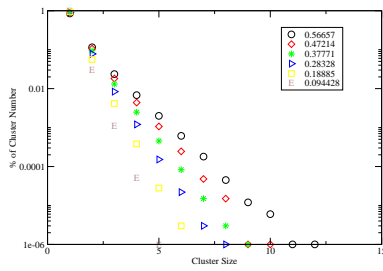


Fig. 11 (a)

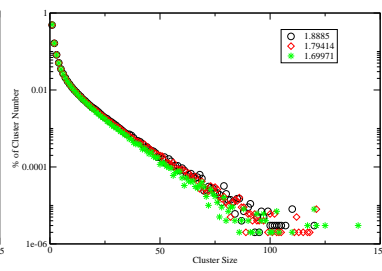


Fig. 11 (d)

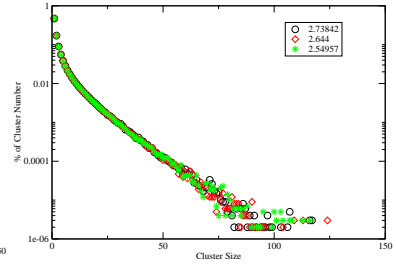


Fig. 11 (g)

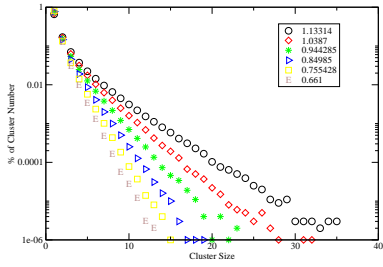


Fig. 11 (b)

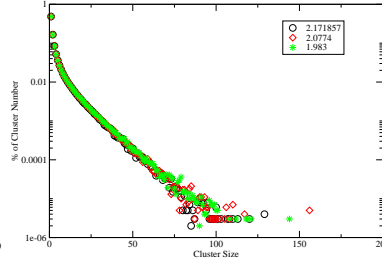


Fig. 11 (e)

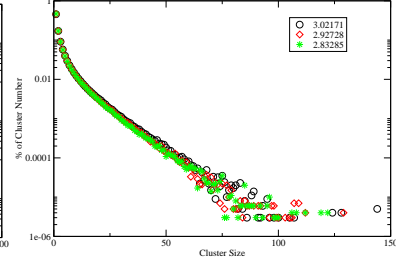


Fig. 11 (h)

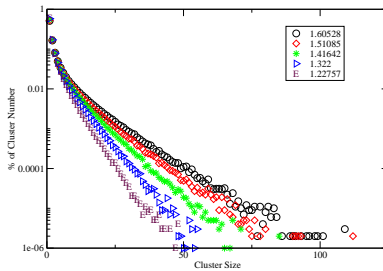


Fig. 11 (c)

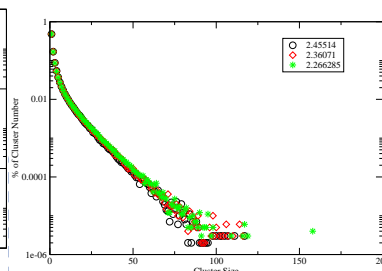


Fig. 11 (f)

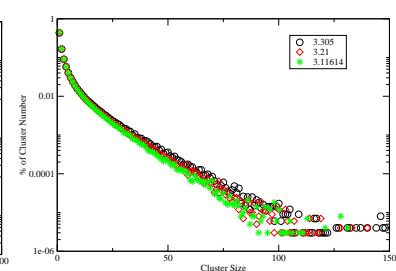


Fig. 11 (i)

Fig. 11 Cluster distributions of the full potential with $K_c=0.5$ and the cutoff of the bond length at $r_{\min}=1.1$

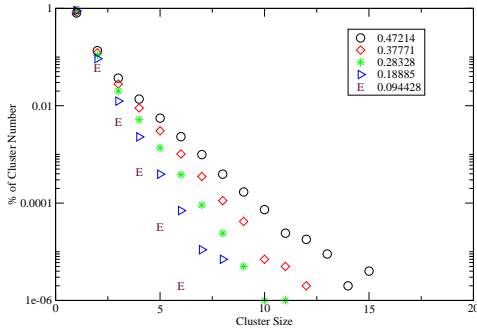


Fig. 12 (a)

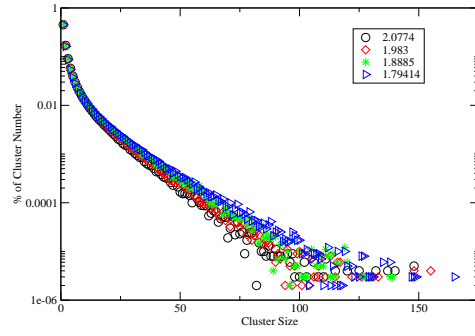


Fig. 12 (e)

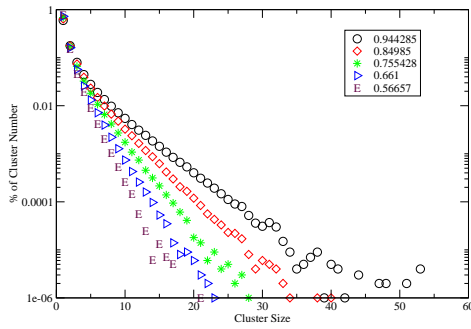


Fig. 12 (b)

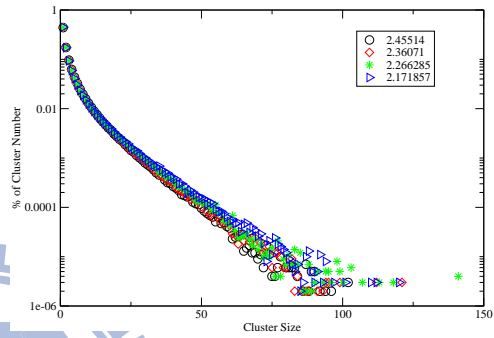


Fig. 12 (f)

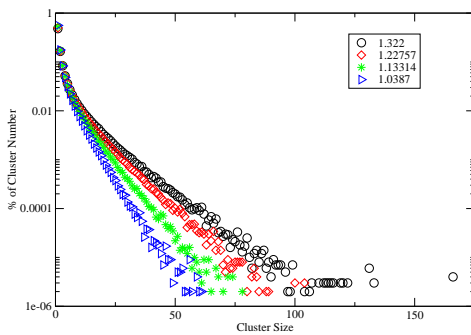


Fig. 12 (c)

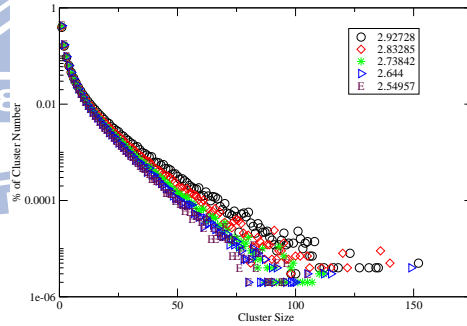


Fig. 12 (g)

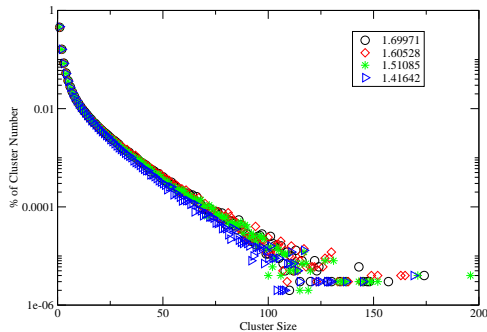


Fig. 12 (d)

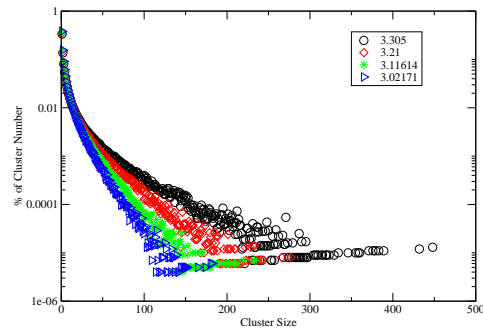


Fig. 12 (h)

Fig. 12 Cluster distributions of the full potential with $K_c=0.5$ and the cutoff of the bond length at $r_{\min}=1.3$

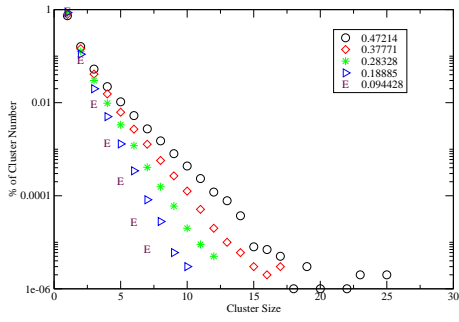


Fig. 13 (a)

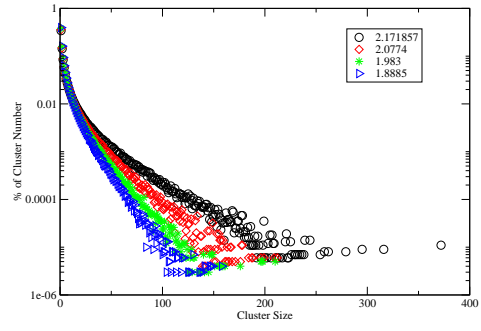


Fig. 13 (e)

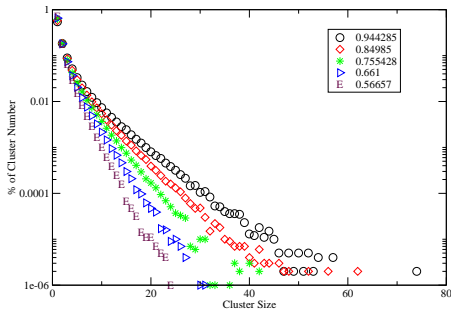


Fig. 13 (b)

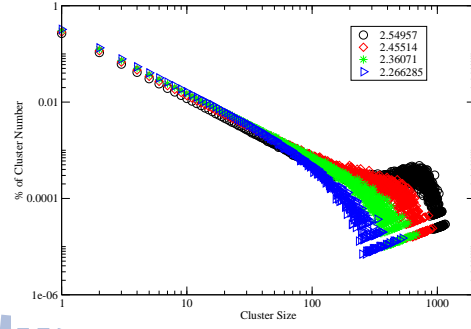


Fig. 13 (f)

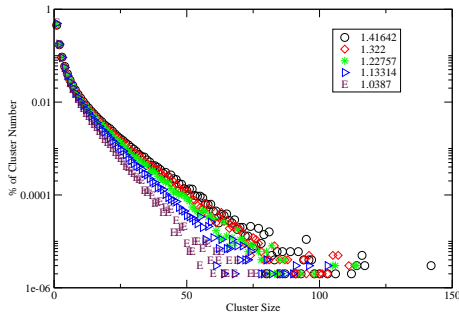


Fig. 13 (c)

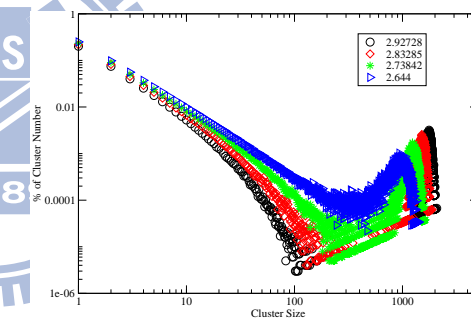


Fig. 13 (g)

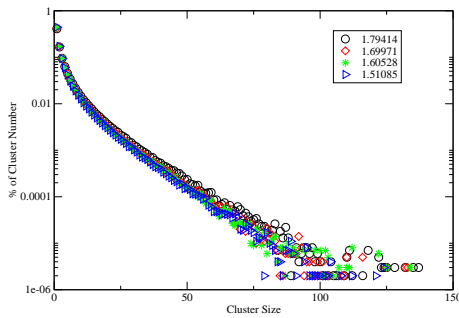


Fig. 13 (d)

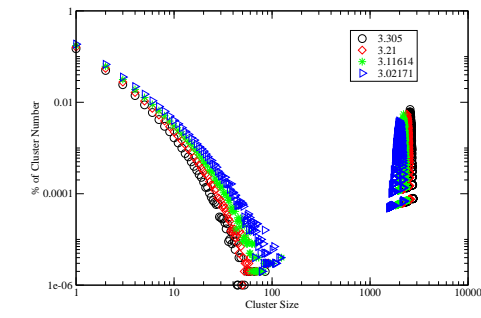


Fig. 13 (h)

Fig. 13 Cluster distributions of the full potential with $K_c=0.5$ and the cutoff of the bond length at $r_{\min}=1.5$

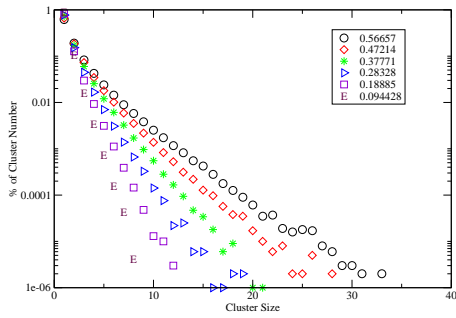


Fig. 14 (a)

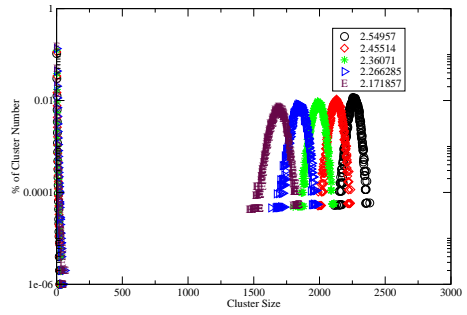


Fig. 14 (e)

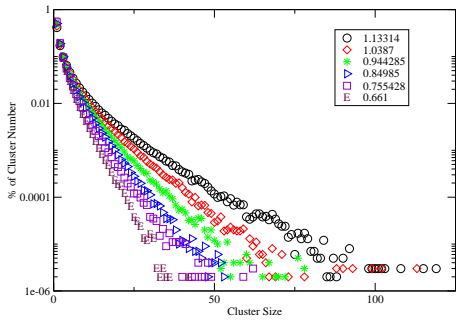


Fig. 14 (b)

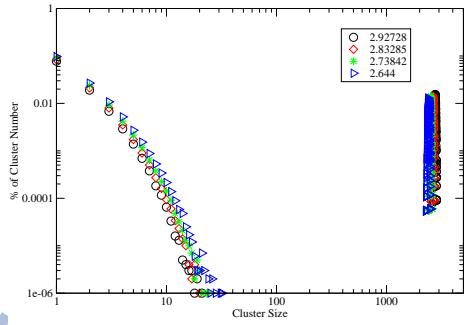


Fig. 14 (f)

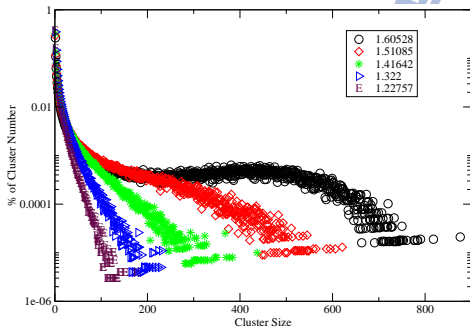


Fig. 14 (c)

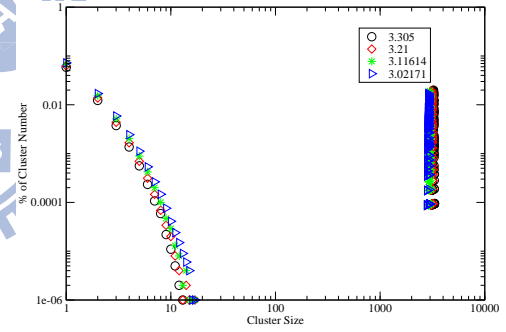


Fig. 14 (g)

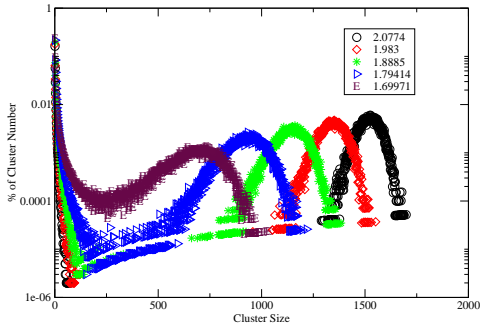


Fig. 14 (d)

Fig. 14 Cluster distributions of the full potential with $K_c=0.5$ and the cutoff of the bond length at $r_{\min}=1.76$

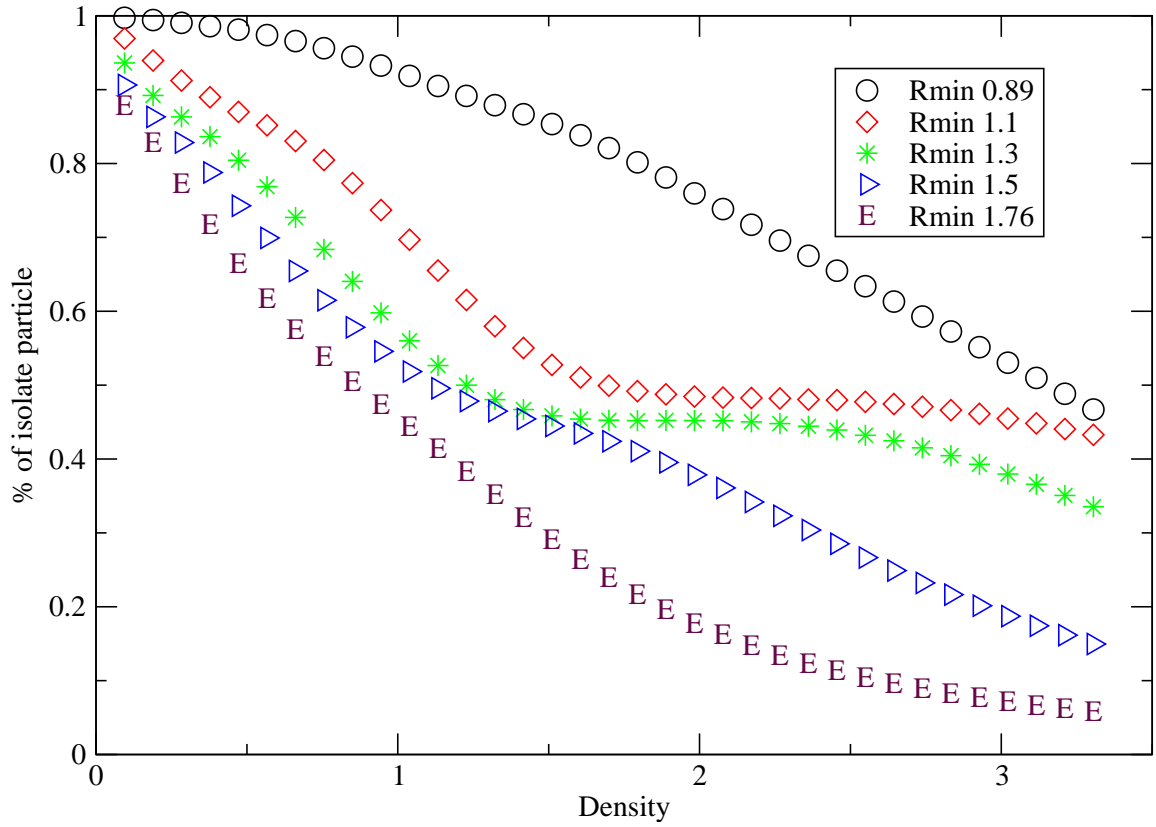


Fig. 15 Density variation of the isolated-particle number for the full potential with the cutoff distance $r_{\min}=0.89, 1.1, 1.3, 1.5$ and 1.76

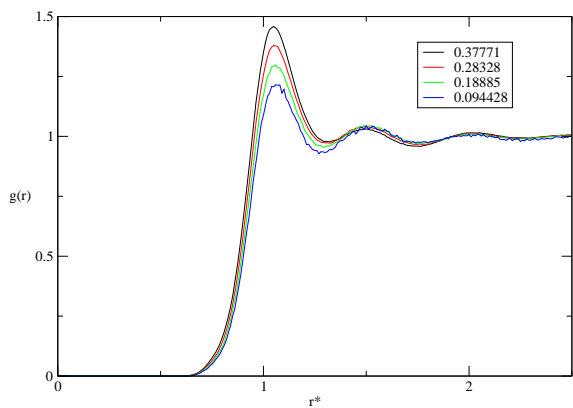


Fig. 16 (a)

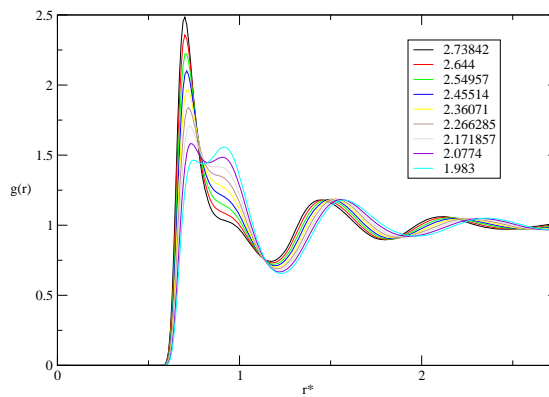


Fig. 16 (d)

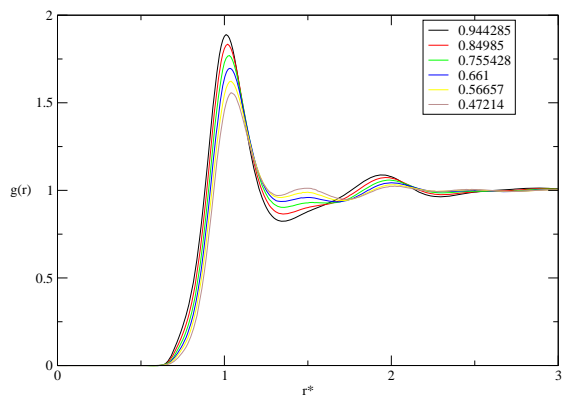


Fig. 16 (b)

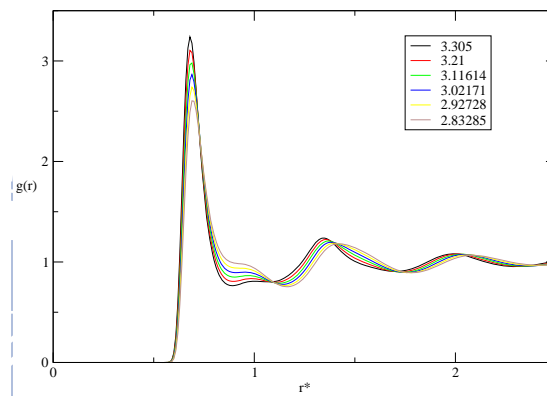


Fig. 16 (e)

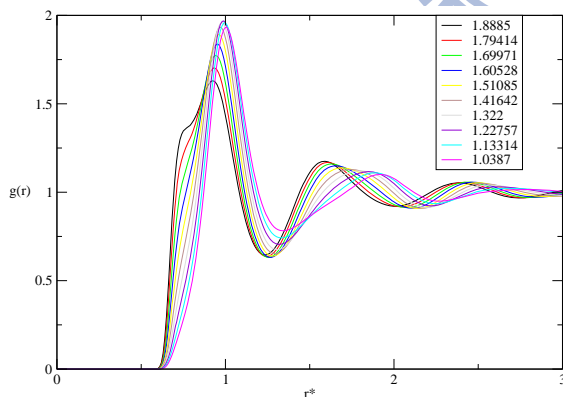


Fig. 16 (c)

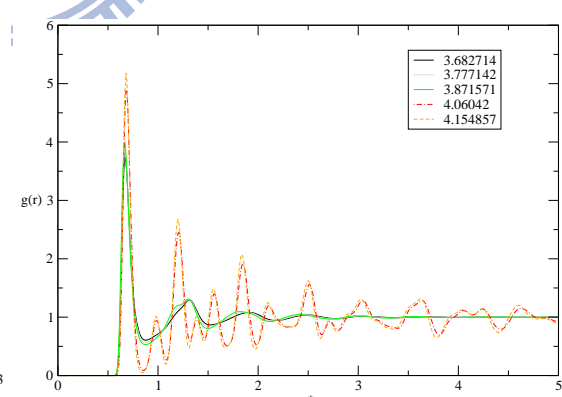


Fig. 16 (f)

Fig. 16 The $g(r)$ function of the full potential at $T=323\text{K}$ and different density

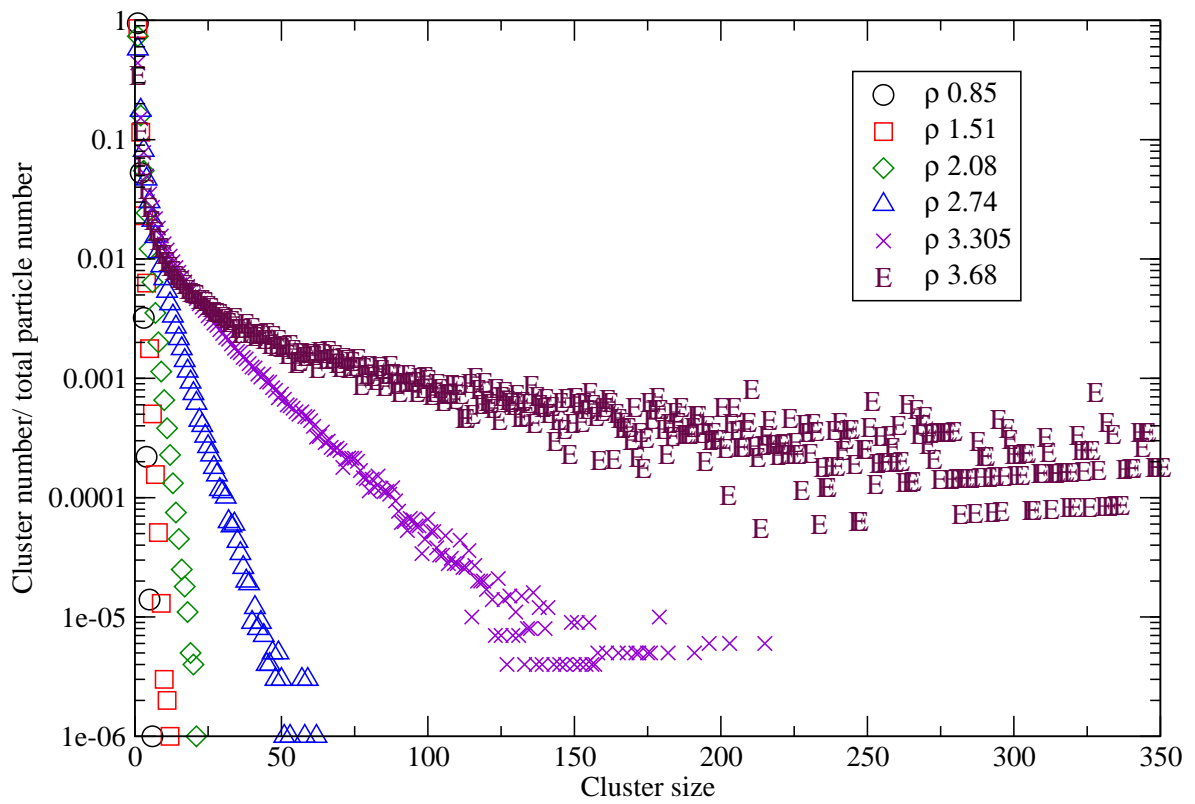


Fig. 17 Cluster distributions of the repulsive core only with $K_c=0.5$ and the cutoff of the bond length at $r_{\min}=0.89$

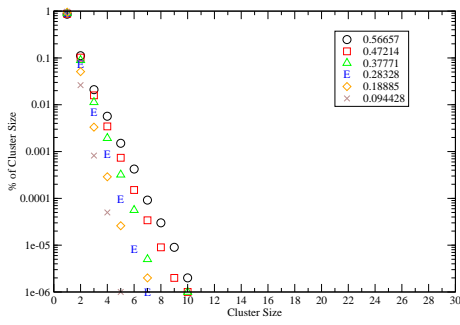


Fig. 18 (a)

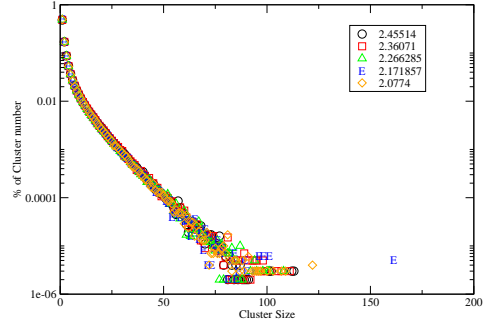


Fig. 18 (e)

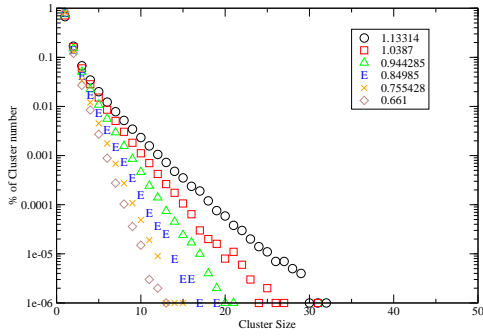


Fig. 18 (b)

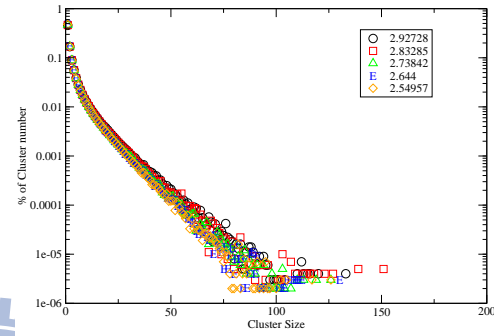


Fig. 18 (f)

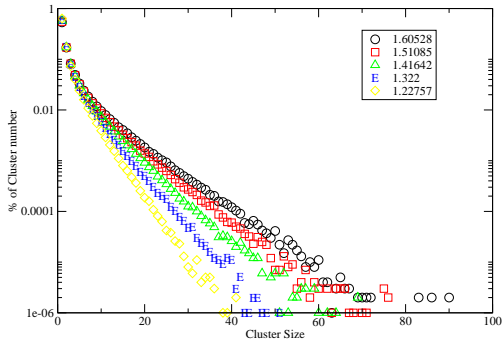


Fig. 18 (c)

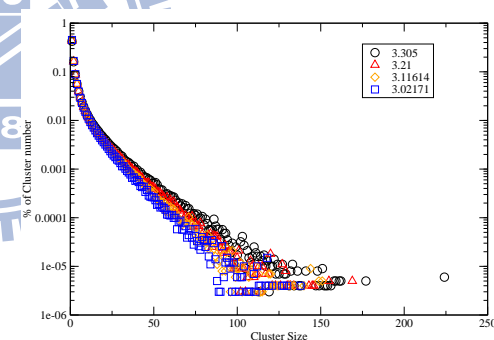


Fig. 18 (g)

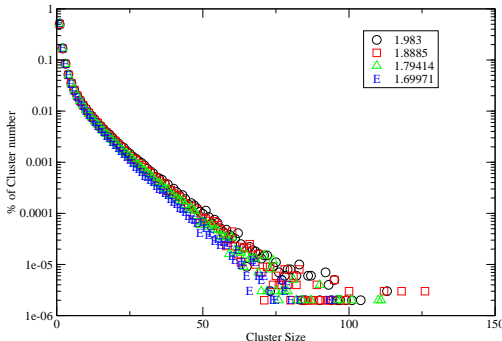


Fig. 18 (d)

Fig. 18 Cluster distributions of the repulsive core only with $K_c=0.5$ and the cutoff of the bond length at $r_{\min}=1.1$

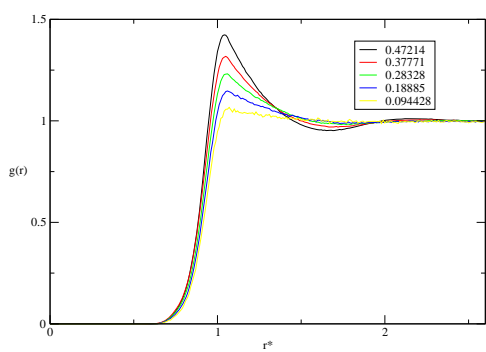


Fig. 19 (a)

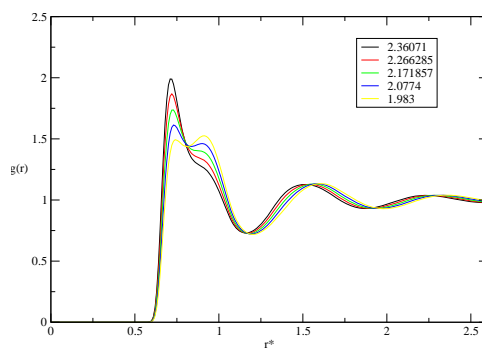


Fig. 19 (e)

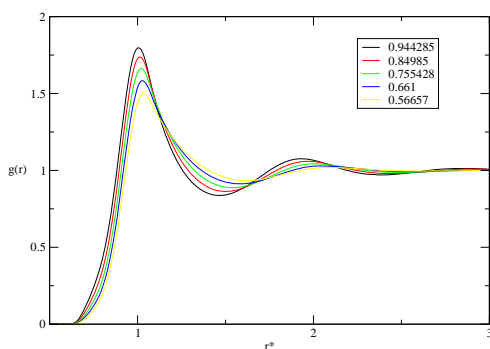


Fig. 19 (b)

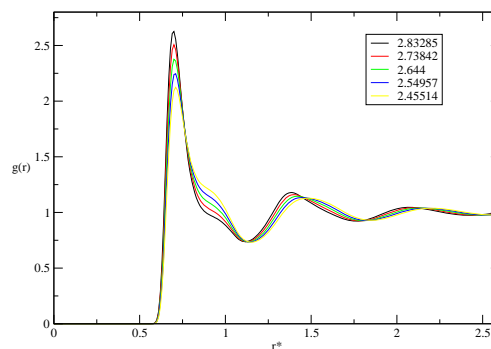


Fig. 19 (f)

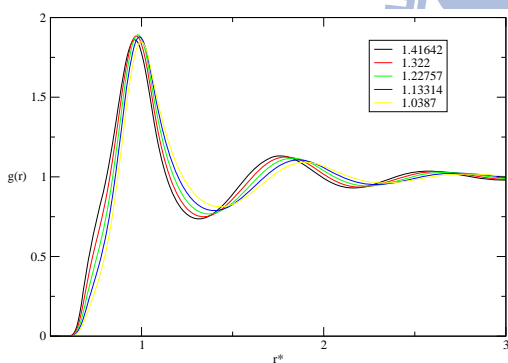


Fig. 19 (c)

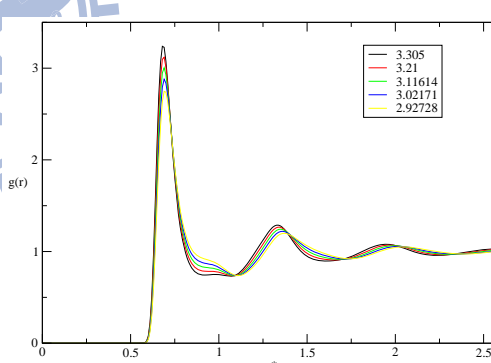


Fig. 19 (g)

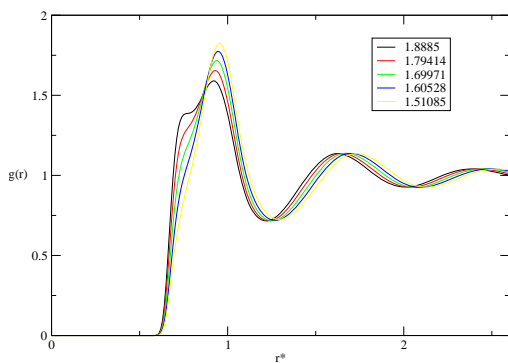


Fig. 19 (d)

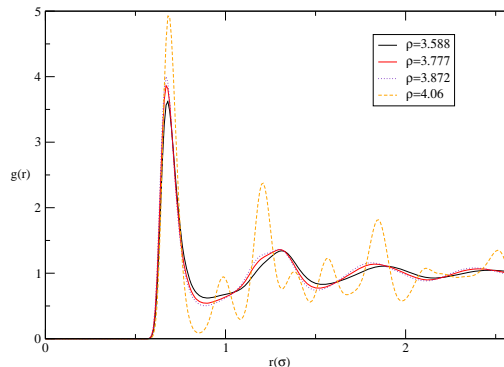


Fig. 19 (h)

Fig. 19 The $g(r)$ function of the repulsive core only at $T=323\text{K}$ and different density

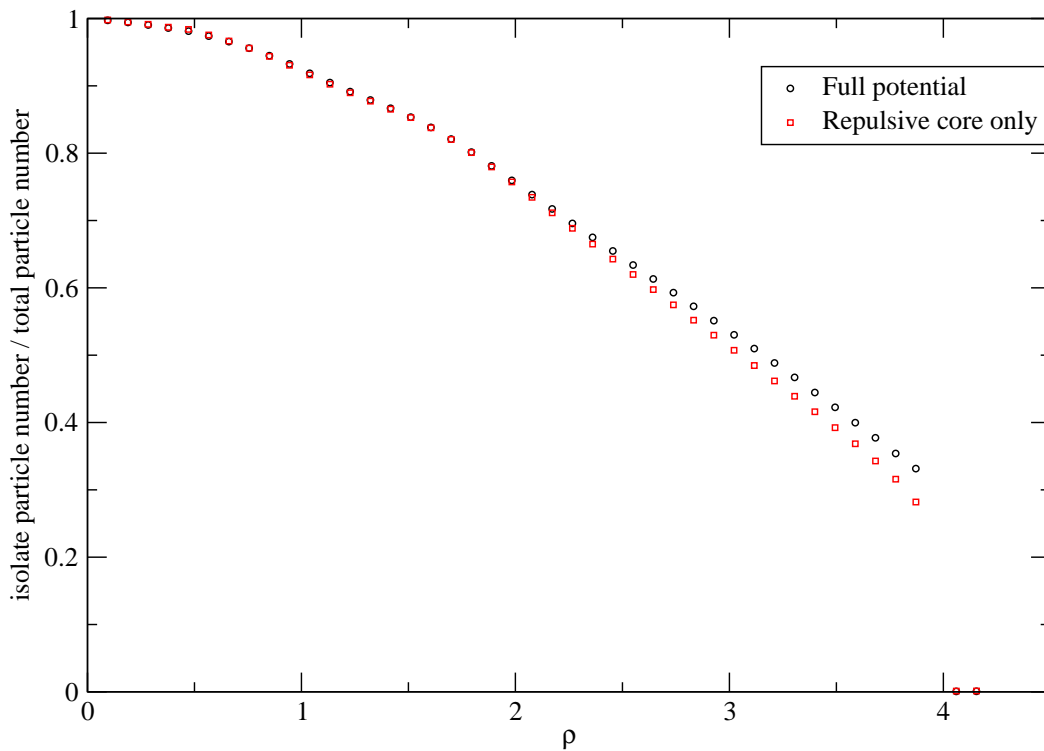


Fig. 20(a)

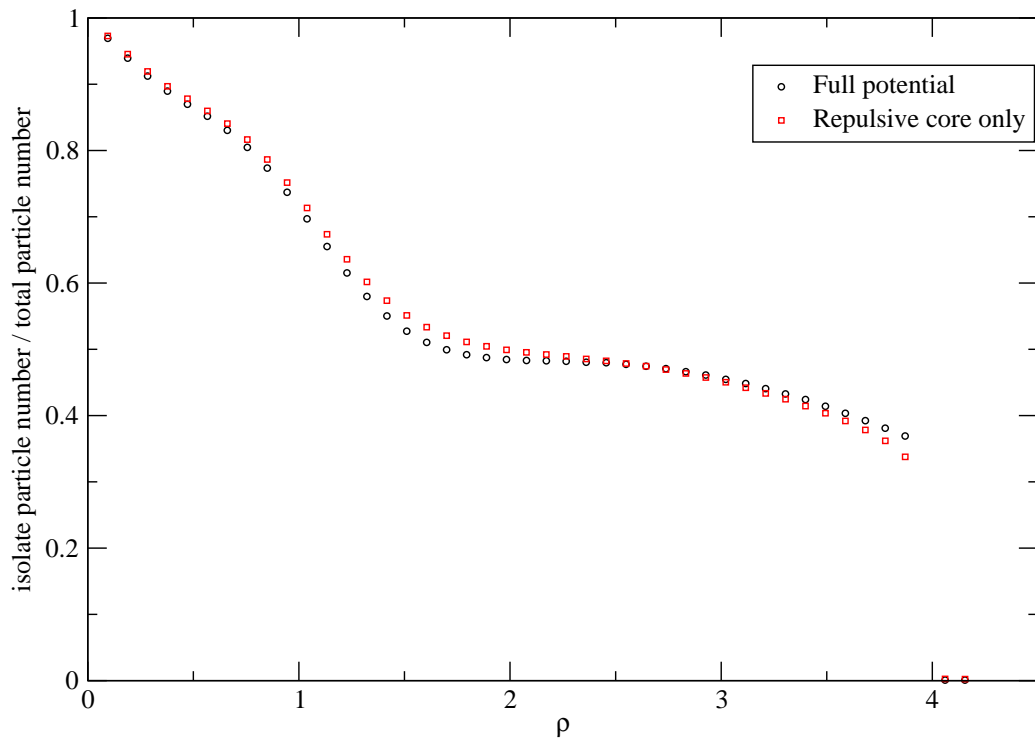


Fig. 20(b)

Fig. 20 Distribution of the isolated particles in the full potential (circles) and the repulsive core only (squares) with $r_{\min}=0.89$ (a) and $r_{\min}=1.1$ (b)

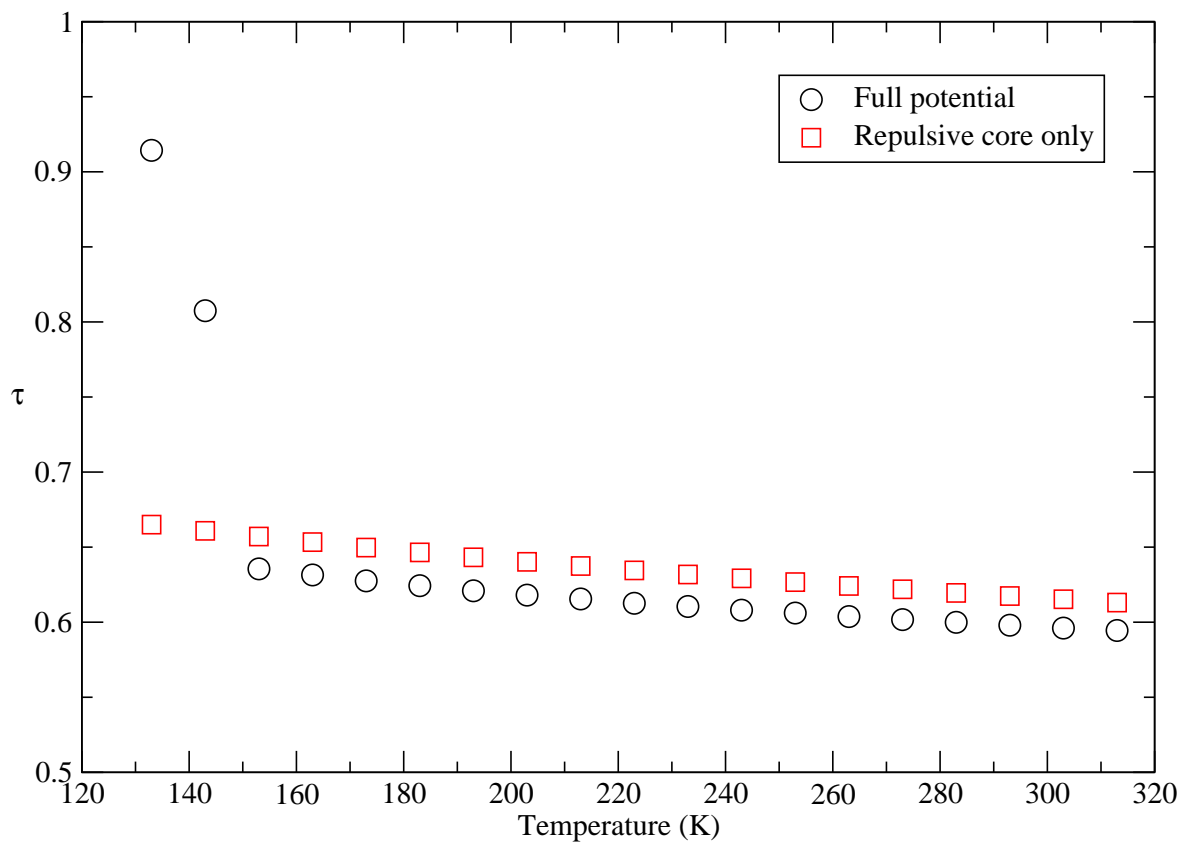


Fig. 21 Temperature variation of the translational order parameter at $\rho = 3.305$ for the models of the full potential (circles) and the repulsive core only (squares)

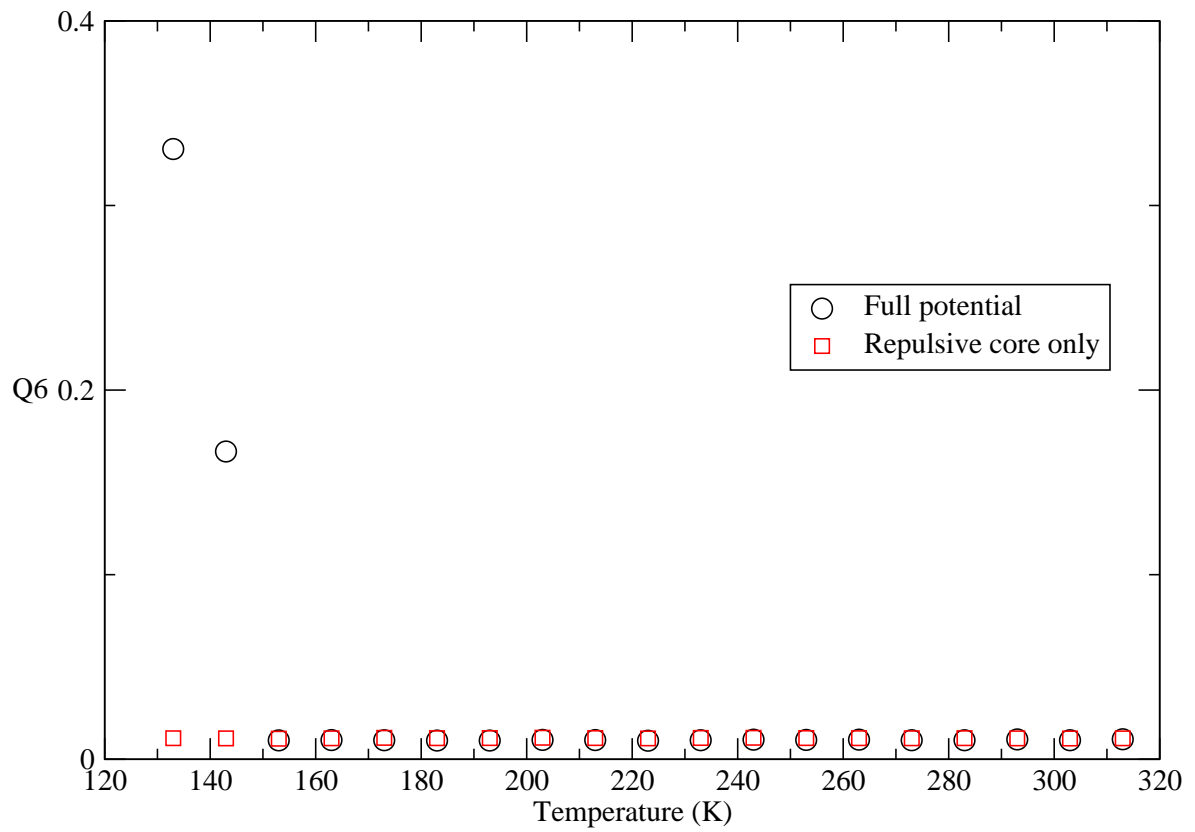


Fig. 22 Temperature variation of the orientational order parameter at $\rho = 3.305$ for the models of full potential (circles) and the repulsive core only (squares)

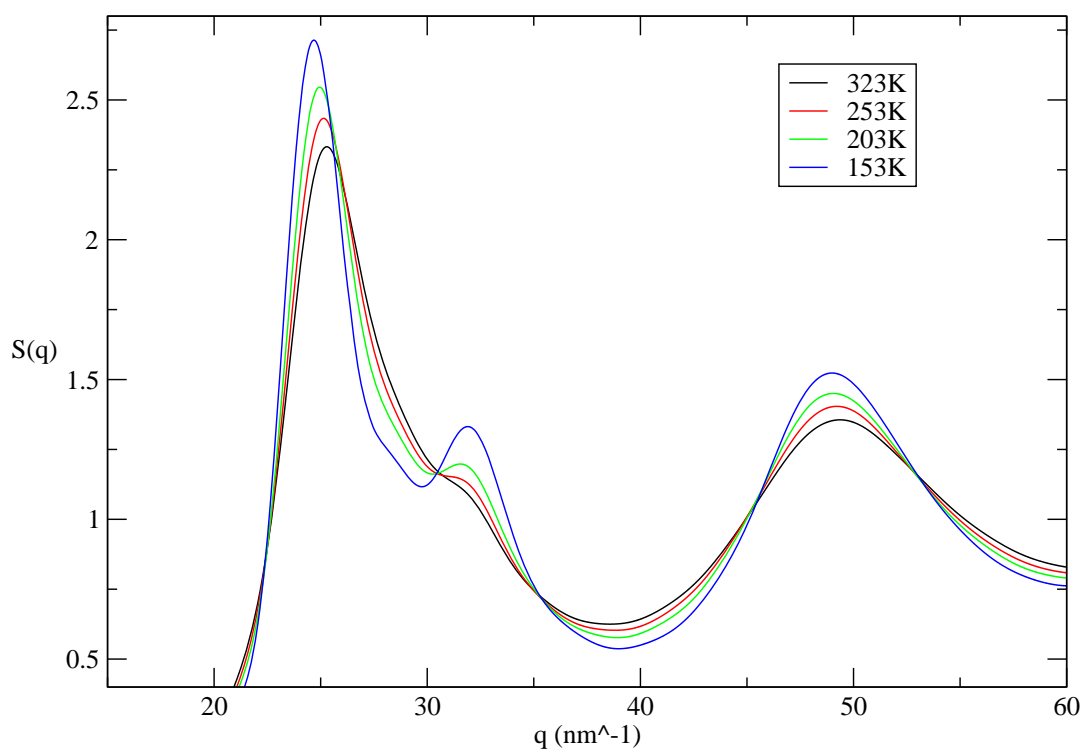


Fig. 23(a)

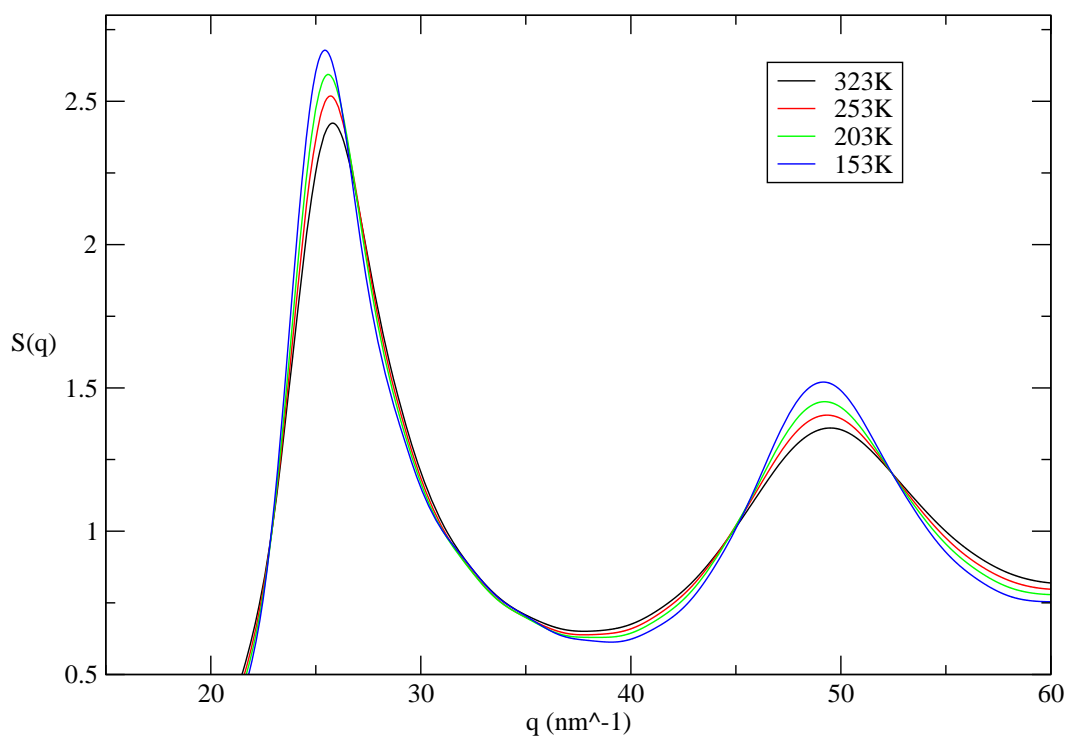


Fig. 23(b)

Fig. 23 Static structure factors $S(q)$ of the full potential (a) and the repulsive core only (b) at $\rho = 3.305$

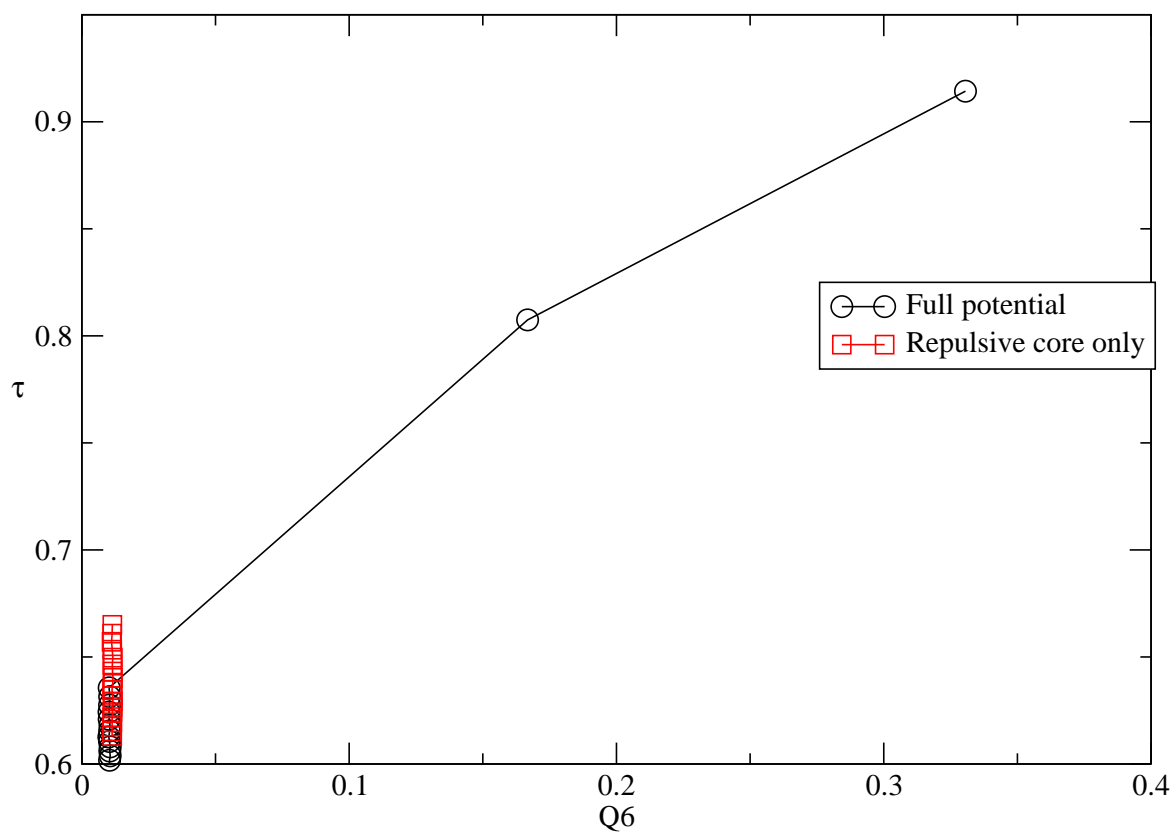


Fig. 24 Order maps for the models of the full potential (circles) and the repulsive core only (squares) at $\rho = 3.305$ and several temperatures

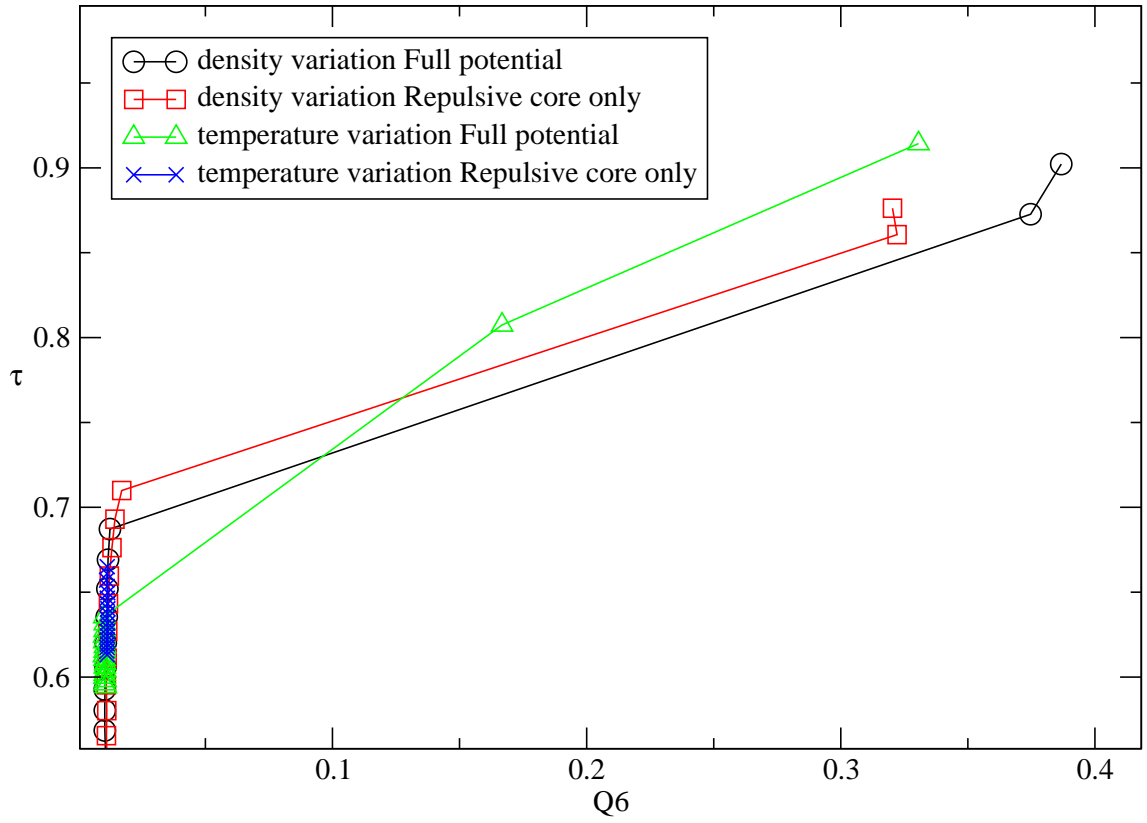


Fig. 25 Comparison for the order map of the temperature and density variations for the models of the full potential and the repulsive core only

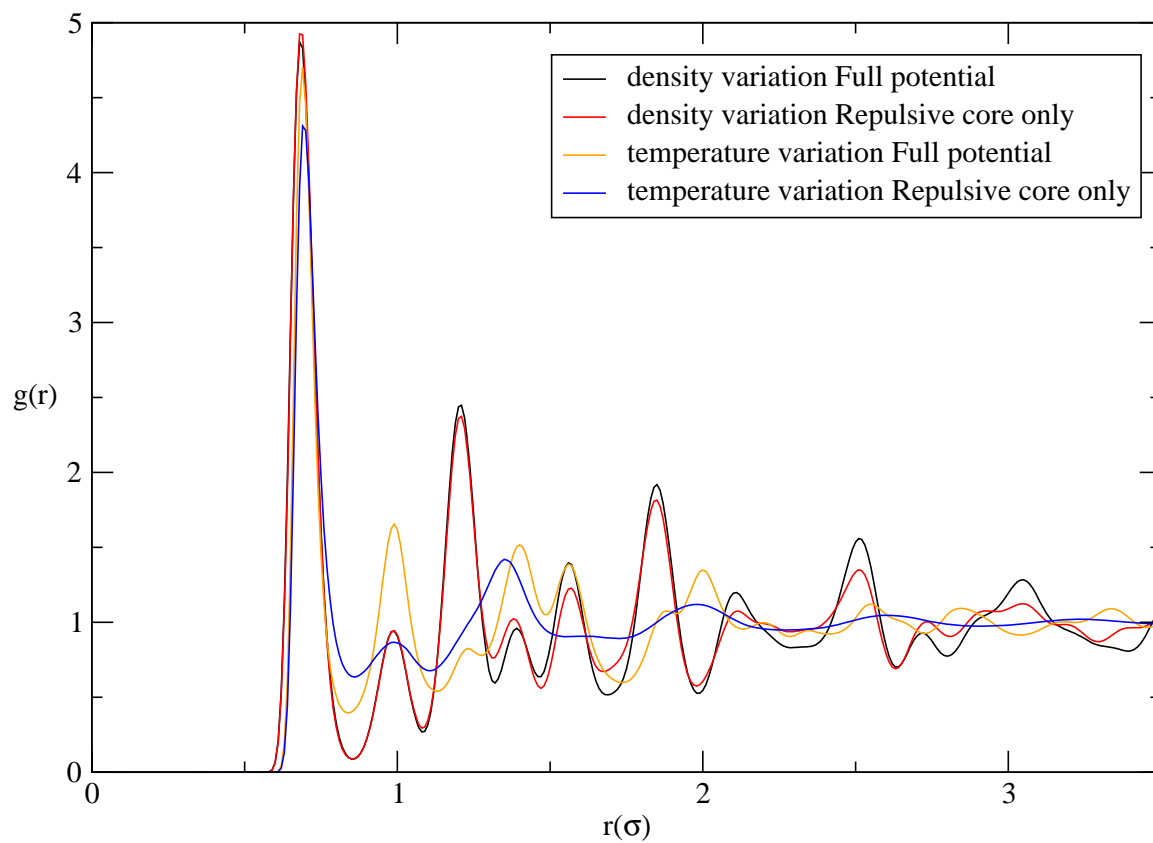


Fig. 26 Comparison for the radial distribution functions $g(r)$ of the solids obtained by different simulation process

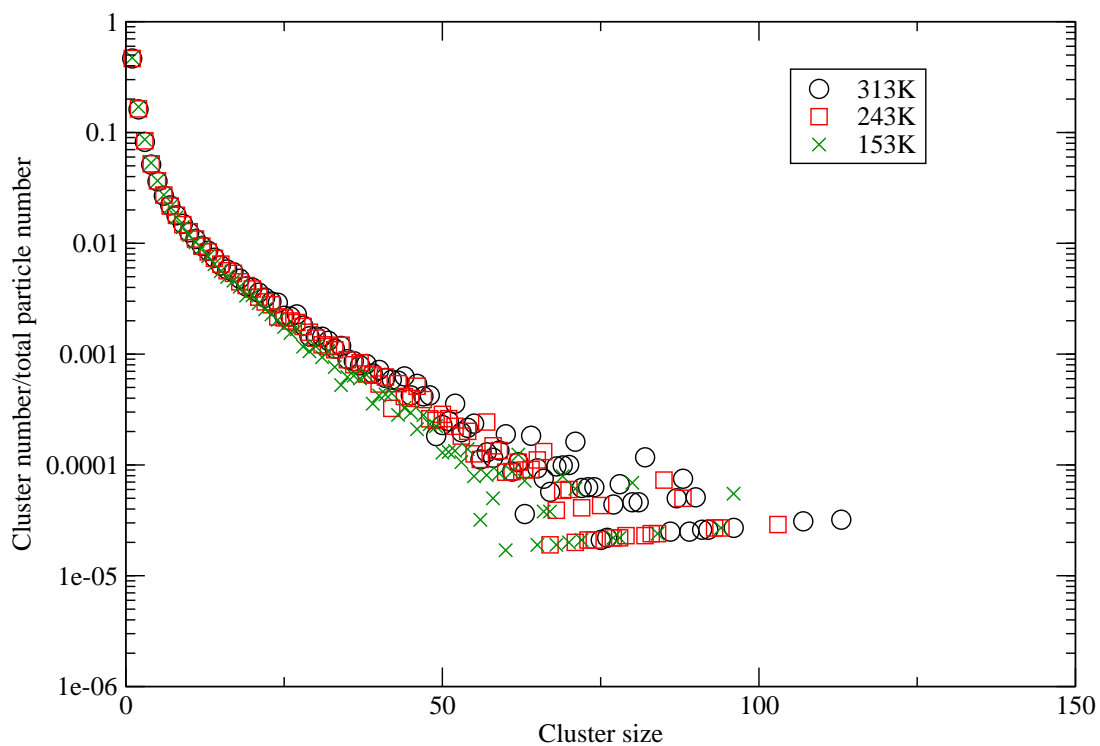


Fig. 27(a)

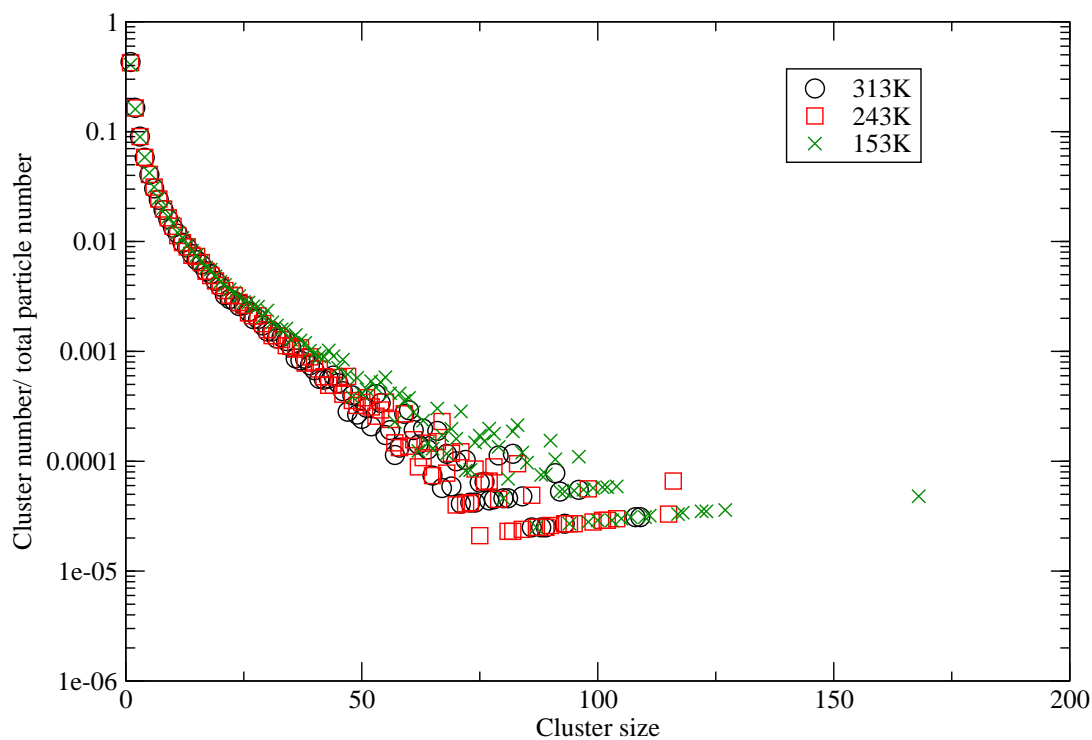


Fig. 27(b)

Fig. 27 The cluster distributions of the full potential at $\rho = 3.305$ and three temperatures with the cutoff $r_{\min} = 0.89$ (a) and $r_{\min} = 1.1$ (b)

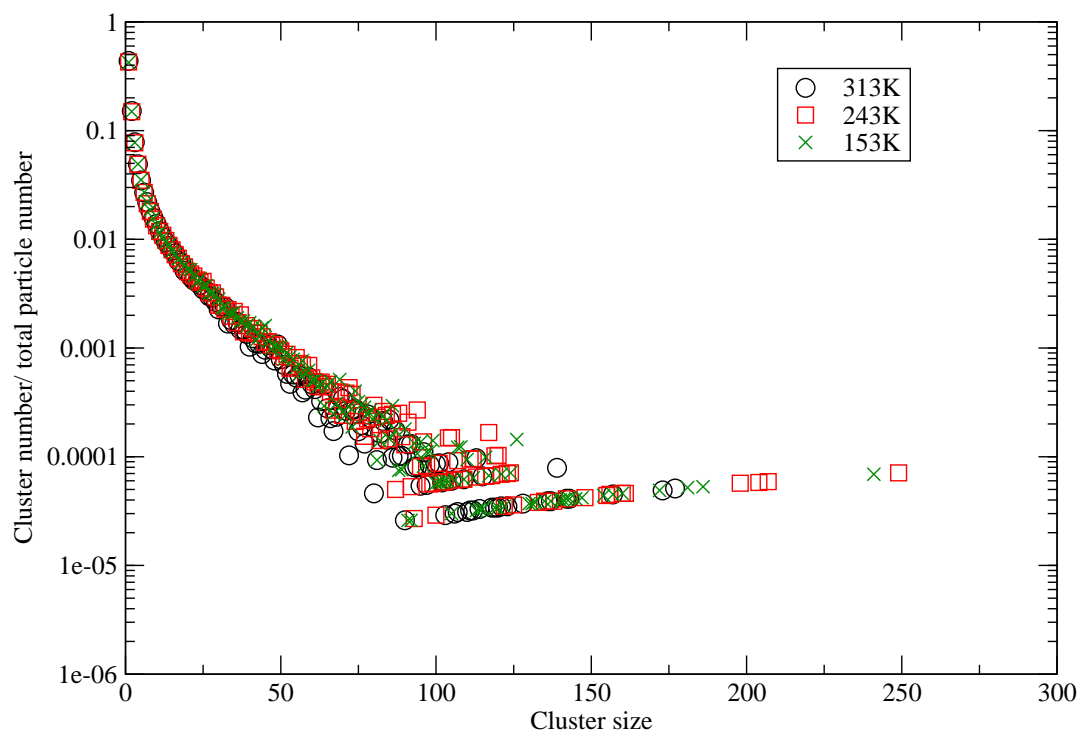


Fig. 28(a)

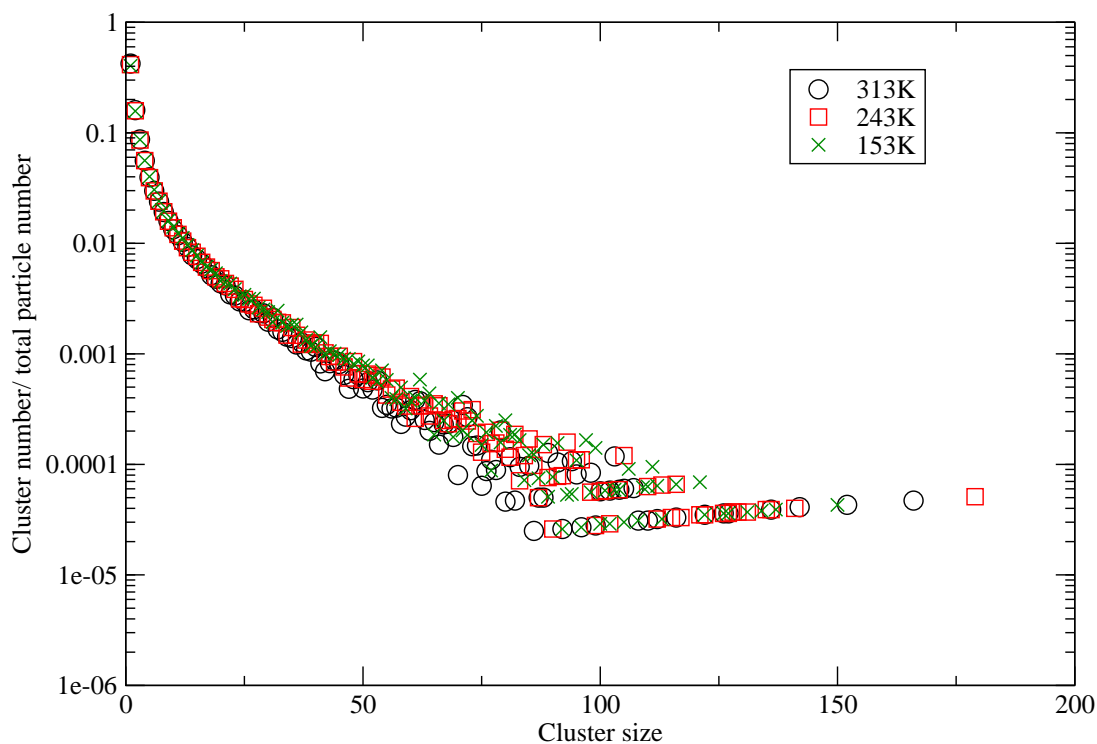


Fig. 28(b)

Fig. 28 The cluster distributions of the repulsive core only at $\rho = 3.305$ and three temperatures with the cutoff $r_{\min} = 0.89$ (a) and $r_{\min} = 1.1$ (b)

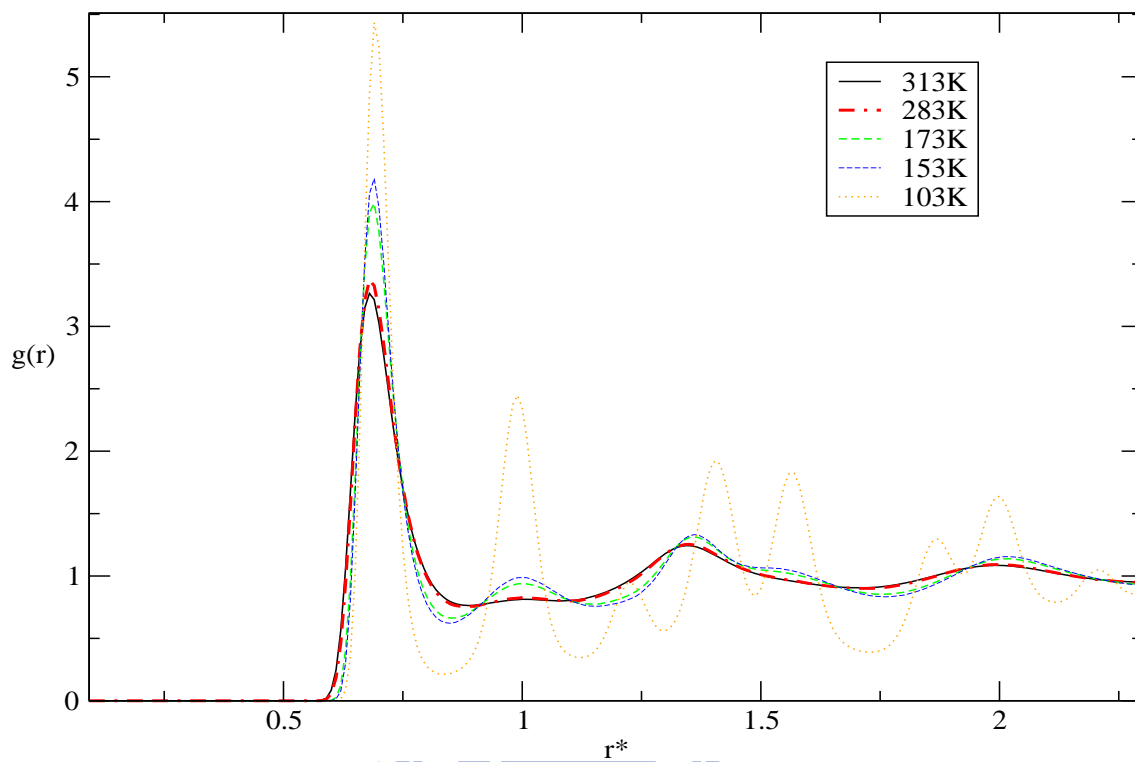


Fig. 29 The $g(r)$ function of the full-potential model at $\rho = 3.305$ and $T = 313\text{k}$, 283K , 173K , 153K and 103K

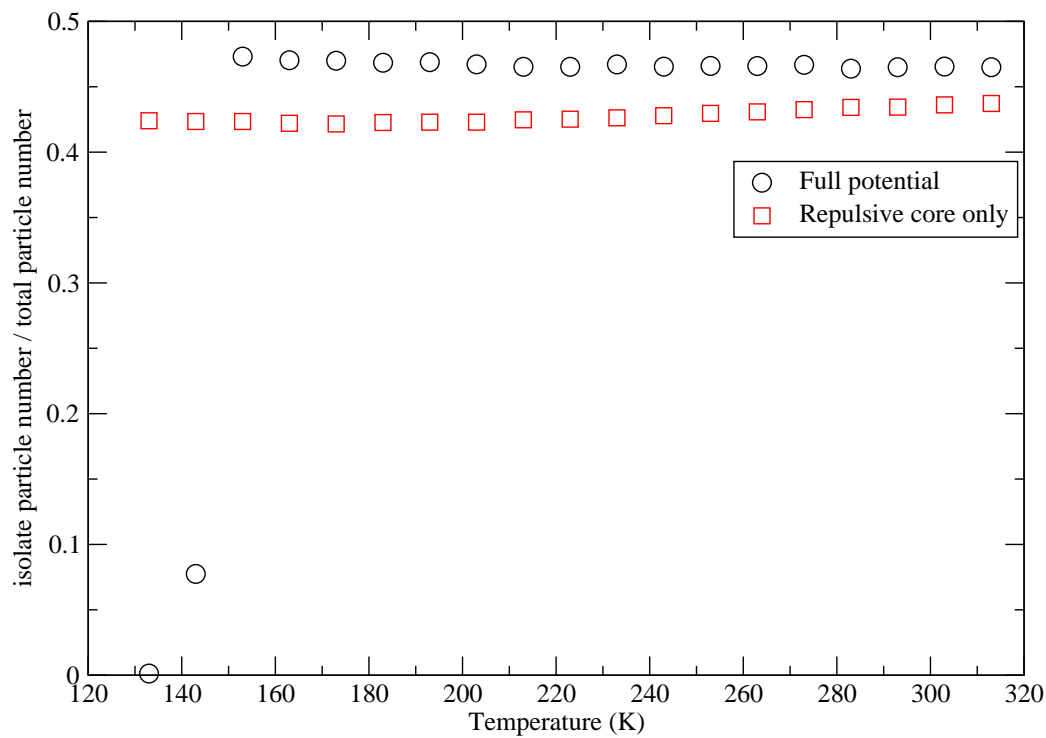


Fig. 30(a)

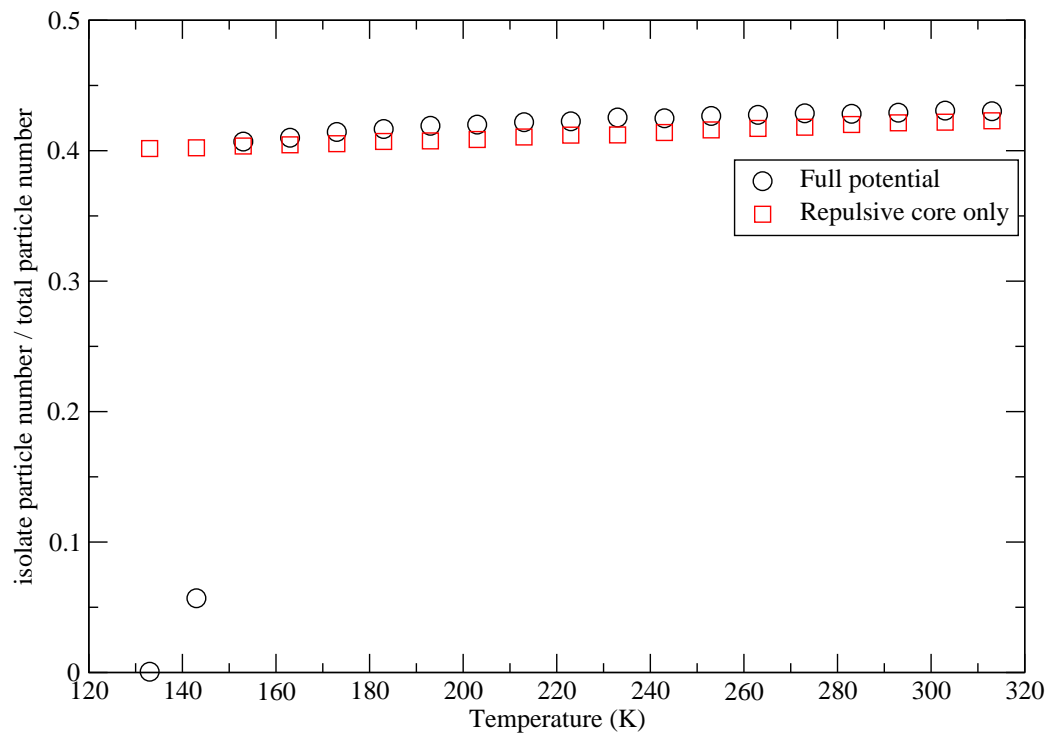


Fig. 30(b)

Fig. 30 Temperature variation of the isolated-particle distribution for the full potential (circles) and the repulsive core only (squares) with the cutoff at

$r_{\min} = 0.89$ (a) and $r_{\min} = 1.1$ (b)

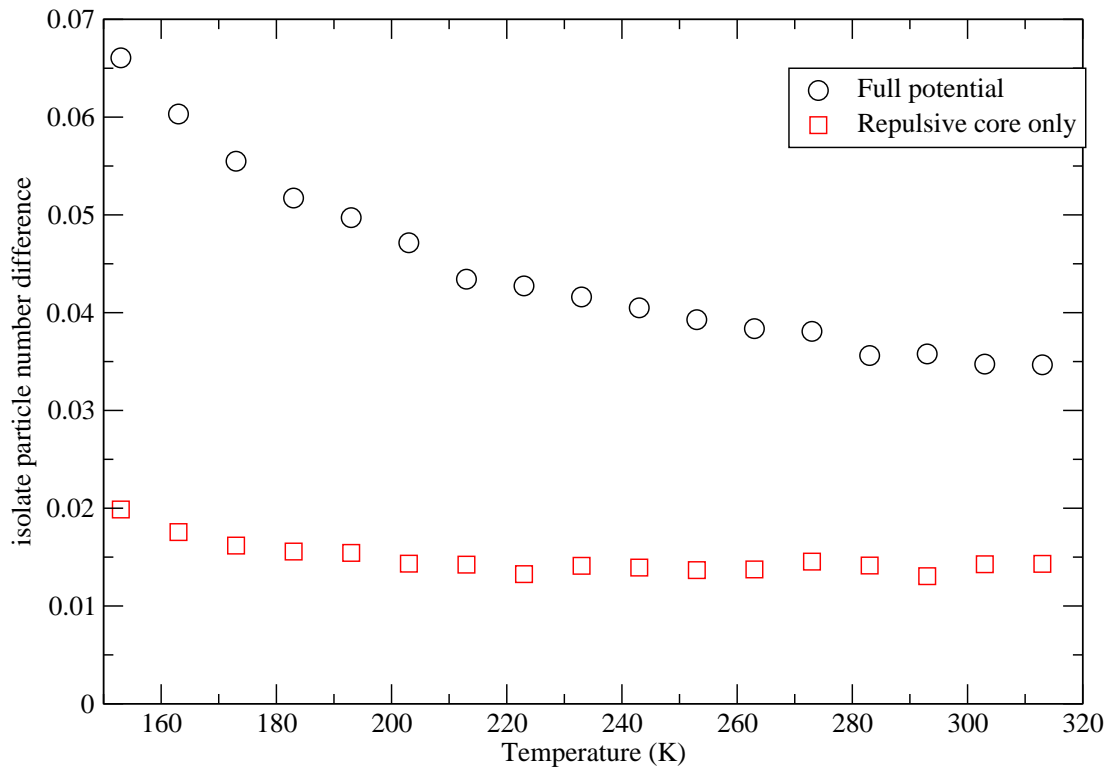


Fig. 31 The difference between the isolated-particle distribution at $r_{\min}=0.89$ and $r_{\min}=1.1$ for the models of the full potential (circles) and the repulsive core only (squares)